

Research Articles | Behavioral/Cognitive

The human cerebellum encodes temporally sensitive reinforcement learning signals

<https://doi.org/10.1523/JNEUROSCI.2313-25.2026>

Received: 19 December 2025

Revised: 5 May 2026

Accepted: 22 May 2026

Copyright © 2026 the authors

This Early Release article has been peer reviewed and accepted, but has not been through the composition and copyediting processes. The final version may differ slightly in style or formatting and will contain links to any extended data.

Alerts: Sign up at www.jneurosci.org/alerts to receive customized email alerts when the fully formatted version of this article is published.

1 **The human cerebellum encodes temporally sensitive reinforcement learning**
2 **signals**

3

4 Juliana E. Trach¹, Yiran Ou¹, & Samuel D. McDougle^{1,2}

5

6 1 – Dept of Psychology, Yale University, New Haven, CT 06510

7 2 – Wu Tsai Institute, Yale University, New Haven, CT 06510

8

9 Correspondence:

10 Juliana E. Trach: juliana.trach@yale.edu

11

12 Keywords: cerebellum; human neuroscience; reinforcement learning; reward prediction
13 error

14 Running title: Reinforcement learning signals in the human cerebellum

15 Main text figures: 5

16 Supplemental figures: 5

17 Abstract: 235 words

18 Introduction: 650 words

19 Discussion: 1495 words

20 **Declaration of interests**

21 The authors have no competing interests.

22 **Acknowledgements**

23 We would like to thank the ACT lab and the other Cog Neuro labs at Yale for helpful
24 discussions about this project. These data were collected at BrainWorks at the WuTsai
25 Institute at Yale University. Thank you to Roeland Hancock and Alex Forrence for
26 technical support at BrainWorks and to Tess Levy, Sanghoon Kang, Laurent Caplette,
27 Lily Behm, Diana Wei, Omri Raccah, and Sophie Allen for support with data collection.
28 JET is supported by the NSF GRFP. SDM is supported by NIH grant number R01
29 NS132926.

30

31

32

33

34 **Abstract**

35 In addition to supervised motor learning, the cerebellum also supports nonmotor forms
36 of learning, including reinforcement learning (RL). Recent studies in animal models
37 have identified core RL signals related to reward processing, reward prediction, and
38 prediction errors in specific regions in cerebellar cortex. However, the constraints on
39 these signals remain poorly understood, particularly in humans. Here, we investigated
40 cerebellar RL signals in a computationally-driven fMRI study. Human participants
41 performed an RL task without low-level sensorimotor contingencies (N = 32, N female =
42 24). We observed robust RL signals related to reward processing and reward prediction
43 errors in cognitive regions of the cerebellum. These signals were not explained by
44 oculomotor or physiological confounds. By manipulating the delay between choices and
45 reward outcomes, we discovered that cerebellar RL signals are temporally sensitive:
46 robust when feedback was delivered shortly following choices, but undetectable at
47 supra-second feedback delays. Similar delay effects were not found in other areas
48 implicated in reward processing, including the ventral striatum and hippocampus.
49 Further, reward prediction error activity in the cerebellum was related to behavioral
50 performance when feedback was delivered promptly, but not when it was delayed.
51 Connectivity analyses revealed that during RL feedback, cognitive areas of the
52 cerebellum coactivate with a network that includes the medial and lateral prefrontal
53 cortex and caudate nucleus. Together, these results highlight a temporally constrained
54 contribution of the human cerebellum to a cognitive learning task.

55

56 **Significance statement**

57 Reinforcement learning (RL) - the shaping of behavior through reward feedback - is an
58 essential cognitive capacity. Previous work has focused almost exclusively on cerebral
59 circuits that support RL, however recent work in animal models also implicates the
60 cerebellum. Despite growing interest in the "cognitive cerebellum," its contributions to
61 human RL remain unclear. We show that regions spanning lobules Crus I/II respond to
62 rewards and encode reward prediction errors in a temporally sensitive manner. Our
63 results build directly on research in model organisms, highlighting functional parallels
64 across species and the importance of crosstalk between human and animal
65 researchers. Including the cerebellum as a node in RL networks creates a potential new
66 target for intervention in cases of reward processing dysfunction, like addiction.

JNeurosci Accepted Manuscript

67 **Introduction**

68 A recent paradigm shift in cerebellar neuroscience recognizes that the
69 cerebellum contributes to both motor control and cognition (Buckner, 2013; Diedrichsen
70 et al., 2019; Diedrichsen & McDougle, 2026; Ito, 2008; Leiner et al., 1986;
71 Schmahmann, 2019; Sokolov et al., 2017; Stoodley et al., 2012; Strick et al., 2009).
72 This shift is motivated by converging lines of evidence: The cerebellum is implicated in
73 cognitive neurodevelopmental disorders (Stoodley, 2016), it is activated by nonmotor
74 tasks (King et al., 2019; Van Overwalle et al., 2014, 2020), damage produces cognitive
75 deficits (Butcher et al., 2017; Drepper et al., 1999; McDougle et al., 2022; Nicholas et
76 al., 2023; Schmahmann & Sherman, 1998; Timmann et al., 2010), and it has
77 bidirectional connections with nonmotor areas of the cerebrum (Bostan et al., 2010,
78 2013; Buckner, 2013; Buckner et al., 2011; Hoshi et al., 2005; Kelly & Strick, 2003; King
79 et al., 2023; Middleton & Strick, 1994; Strick et al., 2009; Wagner & Luo, 2020). Still, a
80 unifying framework of cerebellar function remains elusive. What specific cognitive
81 computations might the cerebellum implement?

82 Some recent work on this question focuses on cerebellar contributions to
83 reinforcement learning (RL; Hull, 2020; Kostadinov & Häusser, 2022). Studies in
84 rodents and nonhuman primates have revealed cerebellar activity encoding core
85 components of RL, including reward processing, reward expectation, and reward
86 prediction errors (Heffley et al., 2018; Kostadinov et al., 2019; Sendhilnathan et al.,
87 2020; Wagner et al., 2017). Such signals have been observed in granule cells (Wagner
88 et al., 2017), climbing fiber inputs (Heffley & Hull, 2019; Kostadinov et al., 2019; Larry et
89 al., 2019), and Purkinje cells (Sendhilnathan et al., 2020), especially in areas spanning

90 lobules Crus I and Crus II (Heffley & Hull, 2019; Sendhilnathan et al., 2020). Moreover,
91 lesion and stimulation studies point to a causal role for the cerebellum in RL (Carta et
92 al., 2019; Huvermann et al., 2025; McDougle et al., 2016; Nicholas et al., 2023). There
93 is now general consensus that the cerebellum supports RL (Manto et al., 2024) in
94 conjunction with circuits in the cerebrum.

95 Still, key gaps remain, especially in human neuroscience. First, there are
96 practical issues: full coverage of the cerebellum with human functional neuroimaging is
97 rarely achieved (Wang et al., 2025), and cerebellar BOLD signals are susceptible to
98 motor and physiological confounds (Diedrichsen et al., 2010; Schlerf et al., 2012;
99 Striener et al., 2015). Second, many RL tasks involve sensorimotor contingencies that
100 blur cognitive and motor components of RL (O'Doherty et al., 2003; Sendhilnathan et
101 al., 2020; Seymour et al., 2004). Finally, specific anatomical localization of RL signals in
102 humans is rarely reported when they are incidentally detected, complicating
103 comparisons to model organisms. These challenges may explain heterogeneity in
104 previously reported cerebellar activations during RL (Garrison et al., 2013; Kruithof et
105 al., 2023; O'Doherty et al., 2003).

106 Theoretical gaps also remain, particularly regarding constraints on cerebellar RL
107 computations. One candidate constraint is temporal sensitivity: In associative motor
108 learning, the cerebellum is optimized for processing rapid cue-outcome intervals (i.e., <
109 ~2 seconds; (Avraham et al., 2022; Brudner et al., 2016; Chettih et al., 2011; Ivry &
110 Keele, 1989; Kitazawa et al., 1995; Smith, 1968), and learning is attenuated when these
111 intervals are exceeded (Gerwig et al., 2008). In contrast, areas like basal ganglia,
112 hippocampus, and neocortex can associate events over longer timescales (Buhusi &

113 Meck, 2005; Foerde & Shohamy, 2011). We thus hypothesize that the cerebellum may
114 be selectively engaged in RL when predictive associations unfold rapidly.

115 We tested this hypothesis using choice behavior, eye-tracking, physiological
116 recordings, and model-based fMRI in humans. Our task avoided low-level sensorimotor
117 associations and we optimized cerebellar coverage. By manipulating delays between
118 choice and feedback, we tested temporal constraints on cerebellar RL signals.
119 Moreover, we used whole-brain fMRI to compare cerebellar RL signals to those in
120 canonical RL regions, to link neural responses to behavior, and to ask if RL feedback
121 drives functional correlations with other regions of the brain.

122 **Methods**

123 ***Participants***

124 Thirty-five individuals participated in the study (Mean age = 22.9 [18-33]; N
125 female = 24). We planned on excluding participants that were not engaging in the task
126 (not responding to >25% of trials or only responding with one response >90% of trials)
127 or that produced too much head motion during the scan (maximum motion over 2.5mm).
128 No participants met our behavioral exclusion threshold. Two participants were excluded
129 for excessive head motion and an additional subject was excluded for technical issues
130 with the data. Our final sample was 32 participants (Mean age = 22.8 [18-33]; N female
131 = 24). The task protocol was approved by the Yale Institutional Review Board.
132 Participants were compensated \$30/hr. They were also told that they could receive up
133 to \$10 bonus payment for their performance in the task to connect the reward feedback
134 during the task to actual reward. We gave all participants the full bonus payment.

135 ***Experimental session***

136 The experimental session was 2hrs long. Participants arrived and were
137 consented and screened for metal. In the scanner, they completed three runs of a
138 probabilistic reinforcement learning (RL) task and three runs of a statistical learning (SL)
139 task (not discussed here). The RL task was always performed before the SL task. Each
140 functional run began with an eye-tracker calibration phase (Eyelink 1000 Plus, Long-
141 range monocular). After the functional runs, we collected a T1 weighted anatomical
142 image before bringing them out of the scanner. Finally, the session concluded with a
143 test phase for the SL task and a debriefing questionnaire. Task and protocol details are
144 explained below.

145 ***Reinforcement learning task***

146 Participants performed three runs of a probabilistic reinforcement learning task in
147 the scanner. During each run, participants saw four pairs of images (8 unique images
148 per run) across trials (**Supplemental Figure 1**). On each trial, they saw one pair of
149 images side-by-side and used an MR-safe, two-button button box with their right hand
150 to select one of the two images (index finger to select left image, middle finger to select
151 right image). They received probabilistic reward feedback (reward: +1 or nonreward: +0)
152 on their response after a delay (Figure 1a). One image in each pair was associated with
153 a .25 reward probability and the other with a .75 reward probability throughout a run of
154 trials. Participants were instructed to select the stimulus on each trial that they thought
155 was most likely to give them points. They were informed that their point total would be
156 translated into a monetary bonus at the end of the session (up to \$10) to motivate them
157 to perform well and ensure that the point-feedback was rewarding. Crucially, the

158 location of each image was counterbalanced across trials so that reward information
159 was associated with the image – the abstract choice – and not with a specific location or
160 motor action.

161 We manipulated the delay between stimulus offset and the presentation of the
162 reward feedback in order to test the hypothesis that the cerebellum would be particularly
163 involved in processing short-latency feedback signals. Participants viewed the pairs of
164 stimuli for 1.5s on each trial, during which time they made their response. Once they
165 made their response, the fixation cross changed color to indicate that their choice had
166 been registered and the stimuli remained on the screen for the remainder of the 1.5s.
167 The stimuli then disappeared and there was a delay before they were presented with
168 reward feedback for 1s. To test the hypothesis that the cerebellum would be sensitive to
169 short-latency feedback, we assigned two pairs in each run to a short feedback delay
170 where the feedback appeared .8s after the stimulus disappeared and the other two pairs
171 to a long feedback delay where feedback appeared after 3s. If they did not respond
172 quickly enough, they received the feedback “Please respond faster.” There was a
173 jittered inter-trial interval (ITI; 1-3s) after feedback presentation.

174 Prior to the three runs of the task, participants executed a short practice block
175 with two pairs of stimuli to orient them to the task. There was no variation in the delay
176 between responses and feedback in the practice block. During the main runs,
177 participants performed 96 trials during a run (24 presentations per pair randomly
178 interleaved). New stimuli were used in each run to prevent participants from using
179 learned values from previous runs.

180 ***Behavioral and physiological analysis***

181 We used participant choices and RTs to characterize their behavior. Trials where
182 participants did not respond were excluded from analysis. Learning was operationalized
183 as the probability of selecting the stimulus associated with the higher reward probability
184 across trials. To quantify learning we implemented a generalized linear model that used
185 iteration (how many times the participant had viewed a specific pair of stimuli) to predict
186 whether or not they chose the higher value stimulus (1 = chose higher value stimulus; 0
187 = chose lower value stimulus). Overall learning was measured as the probability of
188 selecting the higher value stimulus across all trials. We used t-tests to compare overall
189 learning and RTs between short and long delay trials and to compare gaze and
190 biophysiological measures on rewarded versus nonrewarded trials.

191 We additionally collected eyetracking data during the entirety of the scan using a
192 long-range Eyelink 1000 plus. We did not obtain eyetracking data from two participants
193 who used MR-safe glasses during the scan which interfered with tracking and an
194 additional participant due to equipment malfunction. We began each run with a
195 calibration phase. We were primarily interested in differences in gaze behavior on
196 rewarded versus nonrewarded trials that might impact our results. To examine this
197 possibility, we summarized gaze behavior within each trial and at feedback by counting
198 the number of saccades in these time intervals and used a t-test to compare between
199 rewarded and nonrewarded trials.

200 Finally, we collected pulse and respiration data from each participant using
201 Siemens peripheral devices during scanning (samples every 2.5ms). We used a pulse-
202 oximeter positioned on the index finger of the participant's left hand to collect pulse data

203 and a respiration belt positioned around the participant's abdomen to track respiration.
204 A portion of the data was lost due to signal drop out during the task, or subsequent data
205 storage issues. For five additional participants, we excluded their pulse data from our
206 analyses as the pulse-oximeter was unable to acquire a reliable pulse signal. Thus, of
207 the usable runs of functional BOLD data (86 runs across 32 participants), we retained
208 74.4% of the respiration data (64 runs across 24 participants) and 55.8% of the pulse
209 data (48 runs across 18 participants) for analysis.

210 We were primarily interested in whether these physiological metrics varied
211 significantly across rewarded and nonrewarded trials in a way that might impact our
212 results. To test this, we calculated trialwise pulse and respiration rates and then
213 compared these rates on rewarded versus nonrewarded trials. After extracting the data
214 for each metric in each run, we used the *peakdet* function in Matlab (Eli Billauer, 2009)
215 to locate local minima and maxima in the traces. We then calculated a trialwise rate by
216 counting the number of maxima and minima from the onset of the stimuli on one trial to
217 the onset of the stimuli for the next trial and divided that count by the duration between
218 these two time points (in minutes) to determine the rate. We opted to average the
219 number maxima and minima during the time-window-of-interest in this calculation in
220 order to account for situations where a portion, but not all, of a cardiac or respiratory
221 cycle fell within the window of interest. We then calculated subjectwise averages of
222 these rates for rewarded and nonrewarded trials separately and used a t-test to
223 compare the rates.

224 ***Computational modeling***

225 We conducted an RL modeling analysis on subjects' trial-by-trial behavioral data.
226 These models allowed us to bridge our behavioral and neural data through the lens of
227 reinforcement learning theory (Sutton & Barto, 1998). Specifically, we aimed to model
228 subject behavior to estimate latent variables that reflect the core prediction error
229 processes of RL, and then use these computational estimates to explain variance in
230 neural data using model-based fMRI (Cohen et al., 2017). This computational analysis
231 thus allowed us to generate inferred reward prediction error (RPE) time-courses for use
232 in our neural analyses.

233 To model RL behavior and RPEs, we employed a well-established RL model with
234 the basic form:

$$235 \quad (1) \quad Q(s)_{t+1} = Q(s)_t + \alpha \delta$$

$$236 \quad (2) \quad \delta = r - Q(s)_t$$

237 where the value (Q) of a given stimulus (s) that is chosen by the participant on trial t is
238 updated according to the RPE (δ) on that trial (the difference between the expected
239 value Q , and received reward r), with a learning rate parameter α .

240 We compared the fit of three models to participant data. We fit one variant of the
241 model with a single learning rate:

$$242 \quad (3) \quad Q(s)_{t+1} = Q(s)_t + \alpha \delta$$

243 We fit an additional model with separate learning rates (α^+ , α^-) for rewarded
244 versus nonrewarded outcomes (Frank et al., 2007; Trach et al., 2025):

$$245 \quad (4) \quad Q(s)_{t+1} = \begin{cases} Q(s)_t + \alpha^+ \delta & \text{if } r = 1 \\ Q(s)_t + \alpha^- \delta & \text{if } r = 0 \end{cases}$$

246 Finally, because our task consisted of stimulus *pairs*, it is possible that participants may
 247 make counterfactual inferences, such that if one stimulus of the pair was rewarding
 248 them that the other would be unlikely to give them reward, and vice versa (Boorman et
 249 al., 2011). In other words, they may update both the Q value of the chosen stimulus, s ,
 250 and of the unchosen stimulus, s' , when they receive feedback about s . We
 251 operationalized this by adding two additional free parameters that dictated how much
 252 feedback about the chosen stimulus would impact the Q value of the unchosen stimulus
 253 on rewarded and non-rewarded trials:

$$254 \quad (5) \quad Q(s)_{t+1} = \begin{cases} Q(s)_t + \alpha^+ \delta & \text{if } r = 1 \\ Q(s)_t + \alpha^- \delta & \text{if } r = 0 \end{cases}$$

$$255 \quad (6) \quad Q(s')_{t+1} = \begin{cases} Q(s')_t + \omega^+ (0 - Q(s')_t) & \text{if } r = 1 \\ Q(s')_t + \omega^- (1 - Q(s')_t) & \text{if } r = 0 \end{cases}$$

256 Across all models, action selection between the two presented stimuli was
 257 modeled using the softmax function:

$$258 \quad (7) \quad p(s) = \exp(\beta Q(s)) / \sum_i \exp(\beta Q(s_i))$$

259 where β reflects the inverse softmax temperature. We used the MATLAB function
 260 `fmincon` to fit our model to each subject's observed choice data, optimizing the
 261 parameter values to maximize the log posterior probability of the choice data given the
 262 model. During fitting, α , (α^+ , α^-), and (ω^+ , ω^-) were constrained on $[0,1]$ and β on $[0,50]$,
 263 and a Gamma (2,3) prior distribution was used to discourage extreme values of β
 264 (Leong et al., 2017; Trach et al., 2025). Importantly, we fit one of each fitted parameter
 265 per subject rather than fitting new values for each run (i.e., three of each per
 266 participant). The fitted parameters are thus optimized to best reflect participant learning

267 and performance across runs. This approach gives us more data to derive a stable
268 estimate of these parameters for each subject. Further, theoretically, these fitted
269 parameters should reflect psychological variables that remain relatively stable within the
270 task context, and fitting runs separately could lead to overfitting. The fitting procedure
271 was conducted 200 times per subject with randomized starting parameter values to
272 avoid local minima. Simulated choice data (from the optimized model) were produced to
273 investigate and visualize the model's ability to replicate the main behavioral findings,
274 and to generate the trial-by-trial RPE time courses that were fit to the neural data (see
275 below; see also **Supplemental Figure 2**).

276 We compared models using the Bayesian Information Criterion (BIC). This fit
277 metric was implemented here as it balances both goodness of fit with model complexity.
278 Smaller values of BIC are indicative of better model fit. We found that the dual learning
279 rate model was the best fit for participant behavior (one learning rate model: summed
280 BIC = 10,291; dual learning rate model: summed BIC = 9,953; inference model:
281 summed BIC = 10,027; **Supplemental Figure 2**). Thus, we used the dual learning rate
282 model to simulate RPEs for our analyses, though we note that all models produced
283 similar RPE timecourses (**Supplemental Figure 2**). Thus, we used the dual learning
284 rate model in our analyses. Simulated choice data (from the optimized model) were
285 produced to investigate and visualize the model's ability to replicate the main behavioral
286 findings, and to generate the trial-by-trial RPE time courses that were fit to the neural
287 data (see below).

288 ***fMRI acquisition and pre-processing***

289 MR data were acquired with a 3T Siemens Prisma scanner with a 64-channel
290 head coil at BrainWorks at the WuTsai Institute at Yale University. Whole-brain
291 functional images were collected using an echo-planar imaging sequences with
292 Repetition time (TR) = 1000ms, Echo time (TE) = 30ms, voxel size = 2.5x2.5x3 mm³,
293 field-of-view = 20.8 x 20.8 x 20.8 cm³, 48 slices, P to A phase encoding direction, with
294 multi-band acceleration factor = 3 (interleaved) and in-plane acceleration factor = 2.
295 Gradient echo field maps were acquired to correct for distortions due to B0
296 inhomogeneities (acquisition parameters: voxel size = 3 × 3 × 3 mm³, field-of-view = 24
297 × 24 × 24 cm³). We also collected a high-resolution T1 weighted MPRAGE, voxel size =
298 1 mm³, field-of-view = 25.6 × 25.6 × 25.6 cm³. As previously noted, we used Siemens
299 peripherals to track pulse and respiration during the functional runs as well.

300 *Anatomical data preprocessing*

301 Preprocessing was performed using fMRIPrep 23.2.1 (Esteban et al., 2018,
302 2019), which is based on Nipype 1.8.6 (Gorgolewski et al., 2011; Krzysztof J.
303 Gorgolewski et al., 2018). The T1w image was corrected for intensity non-uniformity
304 (INU) with N4BiasFieldCorrection (Tustison et al., 2010), distributed with ANTs 2.5.0
305 (Avants et al., 2008), and used as T1w-reference throughout the workflow. The T1w-
306 reference was then skull-stripped with a Nipype implementation of the
307 antsBrainExtraction.sh workflow (from ANTs), using OASIS30ANTs as target template.
308 Brain tissue segmentation of cerebrospinal fluid (CSF), white-matter (WM) and gray-
309 matter (GM) was performed on the brain-extracted T1w using fast (FSL,
310 RRID:SCR_002823 (Zhang et al., 2001). Brain surfaces were reconstructed using
311 recon-all (FreeSurfer 7.3.2, RRID:SCR_001847, (Dale et al., 1999), and the brain mask

312 estimated previously was refined with a custom variation of the method to reconcile
313 ANTs-derived and FreeSurfer-derived segmentations of the cortical gray-matter of
314 Mindboggle (RRID:SCR_002438, Klein et al., 2017). Volume-based spatial
315 normalization to one standard space (MNI152NLin2009cAsym) was performed through
316 nonlinear registration with antsRegistration (ANTs 2.5.0), using brain-extracted versions
317 of both T1w reference and the T1w template.

318 *Functional data preprocessing*

319 For each of the BOLD runs per subject (across all tasks and sessions), the
320 following preprocessing was performed. First, a reference volume was generated, using
321 a custom methodology of fMRIPrep, for use in head motion correction. Head-motion
322 parameters with respect to the BOLD reference (transformation matrices, and six
323 corresponding rotation and translation parameters) are estimated before any
324 spatiotemporal filtering using mcflirt (FSL, Jenkinson et al., 2002). The BOLD reference
325 was then co-registered to the T1w reference using bbregister (FreeSurfer) which
326 implements boundary-based registration (Greve & Fischl, 2009). Co-registration was
327 configured with twelve degrees of freedom to account for distortions remaining in the
328 BOLD reference. Several confounding time-series were calculated based on the
329 preprocessed BOLD: framewise displacement (FD), DVARS and three region-wise
330 global signals. FD was computed using two formulations following Power (absolute sum
331 of relative motions, Power et al., 2014) and Jenkinson (relative root mean square
332 displacement between affines, Jenkinson et al., 2002). FD and DVARS are calculated
333 for each functional run, both using their implementations in Nipype (following the
334 definitions by (Power et al., 2014). The three global signals are extracted within the

335 CSF, the WM, and the whole-brain masks. Additionally, a set of physiological
336 regressors were extracted to allow for component-based noise correction (CompCor,
337 Behzadi et al., 2007). Principal components are estimated after high-pass filtering the
338 preprocessed BOLD time-series (using a discrete cosine filter with 128s cut-off) for the
339 two CompCor variants: temporal (tCompCor) and anatomical (aCompCor). tCompCor
340 components are then calculated from the top 2% variable voxels within the brain mask.
341 For aCompCor, three probabilistic masks (CSF, WM and combined CSF+WM) are
342 generated in anatomical space. The implementation differs from that of Behzadi et al.
343 (2007) in that instead of eroding the masks by 2 pixels on BOLD space, a mask of
344 pixels that likely contain a volume fraction of GM is subtracted from the aCompCor
345 masks. This mask is obtained by dilating a GM mask extracted from the FreeSurfer's
346 aseg segmentation, and it ensures components are not extracted from voxels
347 containing a minimal fraction of GM. Finally, these masks are resampled into BOLD
348 space and binarized by thresholding at 0.99 (as in the original implementation).
349 Components are also calculated separately within the WM and CSF masks. For each
350 CompCor decomposition, the k components with the largest singular values are
351 retained, such that the retained components' time series are sufficient to explain 50
352 percent of variance across the nuisance mask (CSF, WM, combined, or temporal). The
353 remaining components are dropped from consideration. The head-motion estimates
354 calculated in the correction step were also placed within the corresponding confounds
355 file. The confound time series derived from head motion estimates and global signals
356 were expanded with the inclusion of temporal derivatives and quadratic terms for each
357 (Satterthwaite et al., 2013). Frames that exceeded a threshold of 0.5 mm FD or 1.5

358 standardized DVARS were annotated as motion outliers. Additional nuisance time
359 series are calculated by means of principal components analysis of the signal found
360 within a thin band (crown) of voxels around the edge of the brain, as proposed by
361 Patriat et al. (2017). All resamplings can be performed with a single interpolation step by
362 composing all the pertinent transformations (i.e. head-motion transform matrices,
363 susceptibility distortion correction when available, and co-registrations to anatomical
364 and output spaces). Gridded (volumetric) resamplings were performed using
365 nitransforms, configured with cubic B-spline interpolation. (Copyright Waiver: Much of
366 the above boilerplate text was automatically generated by fMRIPrep with the express
367 intention that users should copy and paste this text into their manuscripts unchanged. It
368 is released under the CC0 license.)

369 *Additional pre-processing after fMRIPrep*

370 The primary aim of this study was to isolate neural correlates of RL within the
371 cerebellum. Thus, we ran planned analyses on masked cerebellar data, in addition to
372 the whole brain. To constrain analyses within the cerebellum and avoid bleed-over from
373 adjacent visual/temporal regions, we masked the cerebellum from functional data
374 aligned to standard MNI space prior to spatial smoothing. Whole-brain and cerebellar-
375 masked data was spatially smoothed with a 5mm kernel. We excluded runs where
376 participants produced any movement over 2.5mm (1 voxel; N = 10 runs) and excluded
377 participants if they did not have multiple runs to contribute (N = 2). One additional
378 participant was excluded due to technical difficulties.

379 **fMRI analysis**

380 *Whole-brain and cerebellar univariate analysis*

381 We modeled BOLD responses using generalized linear models (GLMs)
382 implemented in FSL (version 6.0.7.9). Results from three GLMs are presented in the
383 main text, with additional results from another GLM in the supplement. First, we used a
384 GLM to examine responses to reward versus nonreward feedback. We modeled events
385 as boxcar regressors that lasted for the duration of the event of interest. Regressors of
386 interest were convolved with a double gamma HRF using FSL. Here, we included
387 separate task regressors, in addition to our confound regressors, for 1) choice stimulus
388 appearance, 2) participant response (or delay onset if there was no response), 3) short-
389 delay feedback (with rewarded trials modeled as 1 and nonrewarded trials as -1), and 4)
390 long-delay feedback (with rewarded trials modeled as 1 and nonrewarded as -1). This
391 design meant that main effects of the feedback regressors would highlight regions of the
392 brain that preferentially respond to rewarding versus nonrewarding feedback. Thus,
393 combinations and contrasts of these two regressors can be used to highlight regions of
394 the brain that are sensitive to reward across delays and also regions that are delay-
395 sensitive.

396 We used a model-based approach to locate neural correlates of RPEs and
397 surprise ($|RPE|$) in the brain. To do this, we fit RL models to participant choice data
398 (described above) to obtain participant-specific learning and choice parameters. Then,
399 we used these fitted parameters to simulate trial-by-trial RPEs based on the series of
400 trials that each participant experienced. We included separate parametric regressors for
401 RPEs on short-delay trials versus long-delay trials. In the main version of this model
402 (presented in the main text), we included only rewarded trials in the analysis. Crucially,

403 this allows us to measure true RPE responses that are not confounded with valence. In
404 this model, we additionally included regressors for 1) stimulus appearance, 2)
405 participant response, and 3) the appearance of the feedback. Thus, positive correlations
406 with the RPE regressors should not be due to the appearance of feedback alone or
407 generalized valence responses, but rather with the trial-by-trial variation in inferred RPE.
408 In another version of this model (presented in **Supplemental Figure 3**), we included
409 both rewarded and nonrewarded trials. Here, we included an additional regressor for
410 valence to ensure that correlations with the RPE regressors are not driven by general
411 reward versus nonreward effects (though we note that the valence and RPE regressors
412 are highly colinear, making this model suboptimal). We took a similar approach to
413 examine correlates of surprise. In this case, the parametric regressor was the absolute
414 value of RPEs. Finally, we also leveraged this computational framework to conduct an
415 exploratory analysis examining reward anticipation signals in cerebellum. In this
416 analysis, we used a parametric regressor that had the Q-value of the chosen stimulus
417 for each trial, time-locked to when the shapes were initially presented during the trial. All
418 parametric regressors were z-scored before running the models.

419 We also conducted a whole-brain GLM with task performance as a covariate in
420 the model to assess if RPE signals were related to behavior. Our primary goal was to
421 assess whether cerebellar RPE activity was related to learning for the short-delay pairs.
422 To that end, we quantified performance for the short-delay pairs by calculating the
423 probability of selecting the higher reward probability shape across all presentations of
424 these pairs. We included this metric as a covariate in the group-level analysis for
425 temporally sensitive RPE signals (i.e., the contrast of RPE activity on rewarded trials on

426 short versus long delay trials). We repeated this analysis with performance for long
427 delay pairs and again for the difference in performance between short and long delay
428 pairs.

429 In addition to our regressors of interest, we included a variety of motion and
430 noise regressors in all GLMs. We extracted motion regressors from the fMRIprep
431 pipeline and included six rigid body regressors, a DVARS regressor to account for
432 overall motion, and regressors to scrub high motion (>.5mm) TRs. We included the first
433 10 components of the aCompCor regressors from fMRIprep to account for noise from
434 white matter or cerebrospinal fluid.

435 Runs were combined within-subject before group-level analyses (FLAME 1). We
436 used a cluster-forming threshold of $p < .001$ and a family-wise error cluster-corrected
437 threshold of $p < 0.001$, unless otherwise specified in the text. We additionally present
438 results thresholded at 0 in **Supplemental Figure 4**. For cerebellar-specific analyses we
439 cluster-corrected within the cerebellum. We used nilearn (version 0.8.1) to visualize
440 whole-brain results and the SUIT toolbox (Diedrichsen, 2006; Diedrichsen et al., 2009;
441 Diedrichsen & Zotow, 2015) to visualize cerebellar results on flat maps.

442 *ROI analyses*

443 We conducted additional analyses in *a priori* anatomical ROIs to examine
444 correlates of reward processing and RPE. We used anatomical ROIs from the Harvard-
445 Oxford atlas to create ROI masks. We then extracted subject-wise average β -
446 parameters from the second-level GLM analysis within each mask for each contrast of
447 interest. We used nonparametric bootstrap hypothesis tests to test whether the

448 measured effect was significantly different from zero in each ROI. We opted for these
449 nonparametric tests as they are robust to statistical assumptions necessary for standard
450 parametric tests. For each bootstrap iteration, we randomly sampled from the measured
451 values with replacement to create a distribution. We repeated this process 1,000 times
452 and computed p-values and 95% confidence intervals by comparing the distribution
453 means to the null value (zero in this case).

454 *Psychophysiological interaction (PPI) analysis*

455 We used psychophysiological interaction analyses (Gitelman et al., 2003) to
456 examine task-dependent changes in functional correlations between the cerebellum and
457 cerebrum during feedback processing. This approach examines whether functional
458 coupling between a seed region and other regions of the brain is modulated by
459 experimental factors. We first extracted a time series of activation from our two *a priori*
460 cerebellar lobular ROIs (Crus I and Crus II) as the physiological regressors in this
461 analysis. Then, we constructed the psychological regressor that identified feedback
462 epochs in the task versus other trial epochs (e.g., stimulus appearance, delay etc.)
463 which was convolved with a canonical hemodynamic response function. Finally, we
464 created a regressor that reflected the interaction of the physiological and psychological
465 regressors. This regressor reveals regions of the brain that significantly covary with the
466 seed region specifically during the epochs of interest.

467 ***Data and code availability statement***

468 Processed data and code will be available upon publication of the manuscript.

469 **Results**

470 *Human Crus I and Crus II preferentially respond to reward feedback*

471 Participants (N=32) performed a probabilistic reinforcement learning (RL) task
472 while undergoing fMRI. Participants observed two stimuli on each trial and used a
473 button box to select the stimulus (left or right) that they thought was most likely to yield a
474 reward (**Figure 1a**). Their goal was to win points to earn a monetary bonus at the end of
475 the task. After they made their choice, there was a delay period (short delay: 0.8s; long
476 delay: 3s) before they received probabilistic reward feedback (nonrewarded trials: +0;
477 rewarded trials: +1) which they could use to guide future choices. Participants saw four
478 distinct pairs of stimuli within each run (see *Methods* and **Supplemental Figure 1**). In
479 each pair, one stimulus was associated with a .75 probability of reward and the other
480 with a .25 probability of reward. Importantly, the location of the stimuli was randomized
481 across trials, such that rewards were associated with the abstract stimulus choice rather
482 than a specific motor action or spatial location. Our *a priori* regions of interest (ROIs)
483 were Crus I and Crus II in the cerebellum (following work in nonhuman primates
484 (Sendhilnathan et al., 2020) and rodents (Heffley & Hull, 2019)), and canonical
485 subcortical RL regions in nucleus accumbens (NAc), caudate nucleus (Cd), and
486 hippocampus (Hpc; **Figure 1b**).

487 Participants performed the RL task well, showing significant learning across trial
488 blocks (GLM: choose correct ~ iteration + (1|subject); iteration: $b = 0.026$, $SE = 0.0037$,
489 $z = 6.93$, $p < .001$; **Figure 1c**; see also **Supplemental Figure 2**). These learning data
490 were fit with an RL model which was used for later model-based fMRI analyses (see

491 *Methods*). Importantly, the plateau in the performance curve does not mean that
492 participants were only actively learning early in the block - their performance plateaued
493 at choosing the more rewarding stimulus on 73.8% of trials in the last five iterations of
494 each stimulus pair, rather than 100% which would be the optimal behavior. Additionally,
495 because reward feedback was probabilistic, participants will continue to experience
496 prediction errors throughout the block.

497 At the group level, feedback delay did not significantly affect choice behavior or
498 reaction times (p(choose higher value stimulus): $t(31) = 0.51$, 95% CI = [-0.02, 0.04], $p =$
499 .616; RT: $t(31) = 0.03$, 95% CI = [-0.01, 0.01], $p = .976$; **Figure 1d**). Crucially, there was
500 comparable gaze behavior (**Figure 1e**; at feedback: N saccades: $t(28) = 0.76$, 95% CI =
501 [-0.05, 0.11], $p = .451$) and physiological measures (**Figure 1f**; rewarded versus
502 nonrewarded trials: respiration: $t(23) = -0.95$, 95% CI = [-0.37, 0.14], $p = .353$; pulse:
503 $t(18) = 1.27$, 95% CI = [-0.25, 0.83], $p = .274$) on rewarded versus nonrewarded trials,
504 meaning that our key neural analyses would not be significantly confounded by these
505 factors. (This is an important control, as confounding factors like eye movements can
506 influence cerebellum activity.)

507 For our neural analyses, we first used generalized linear models (GLMs) to
508 examine activity between rewarded and nonrewarded trials. In addition to canonical
509 reward processing regions (**Figure 2a, left panel**), we also observed significant activity
510 in the lateral cerebellum around the Crus I/Crus II boundary that reflected greater
511 feedback responses on rewarded versus nonrewarded trials (**Figure 2a, right panel**).
512 The localization of these signals broadly corresponds with previously reported effects in

513 both rodents (Heffley & Hull, 2019) and nonhuman primates (Sendhilnathan et al.,
514 2020).

515

516 *Cerebellar reward signals are temporally constrained*

517 We next tested whether these cerebellar signals were affected by feedback
518 delay. We hypothesized that the cerebellum would be specifically responsive to
519 feedback on short-delay (0.8s) versus long-delay (3s) trials, echoing temporal
520 constraints on cerebellar processing in motor learning tasks (Brudner et al., 2016;
521 Cheng et al., 2008; Kitazawa et al., 1995). We thus examined responses to rewards at
522 short- and long-delay intervals separately. In line with our hypothesis, we found
523 significant cerebellar responses to rewards on short-delay, but not long-delay, trials
524 (**Figure 2b**; see **Supplemental Figure 5**). Activity was primarily localized to Crus I and
525 Crus II. The null findings on long delay trials held even with a relaxed statistical
526 threshold (cluster-corrected in cerebellum, $p < .05$), indicating that the lack of significant
527 reward responses at long delays was not simply a result of conservative thresholding.

528 We additionally asked whether this temporal sensitivity was specific to the
529 cerebellum, or was also reflected in other reward processing regions (NAc, Cd, and
530 Hpc; (Foerde & Shohamy, 2011)). We extracted β -values for the rewarded >
531 nonrewarded contrast (**Figure 2c**; see also **Supplemental Figure 5** for main effects of
532 reward versus non-reward feedback) from these ROIs at short and long delays.
533 Corroborating the whole cerebellum results, the *a priori* anatomical cerebellar ROIs only
534 exhibited significant positive responses at short delays (nonparametric bootstrap test:

535 short delays: Crus I: $M = 0.32$, 95% CI = [0.19, 0.45], $p < .001$; Crus II: $M = 0.29$, 95%
536 CI = [0.16, 0.42], $p < .001$; long delays: Crus I: $M = -0.09$, 95% CI = [-0.26, 0.10], $p =$
537 .346; Crus II: $M = 0.02$, 95% CI = [-0.15, 0.19], $p = .844$). This pattern of results in
538 cerebellum was driven by significant positive activity during feedback on short delay
539 trials (**Supplemental Figure 5**; nonparametric bootstrap test: Crus I: short-delay reward
540 effect: $M = 0.51$, 95% CI = [0.33, 0.68], $p < .001$; short-delay no-reward effect: $M = 0.28$,
541 95% CI = [0.12, 0.44], $p < .001$; Crus II: short-delay reward effect: $M = 0.31$, 95% CI =
542 [0.08, 0.53], $p = .006$; short-delay no-reward effect: $M = 0.07$, 95% CI = [-0.10, 0.24], $p =$
543 .045) and negative activity on long delay trials whose magnitude was invariant to the
544 valence of the feedback (nonparametric bootstrap test: Crus I: long-delay reward effect:
545 $M = -0.44$, 95% CI = [-0.64,-0.24], $p < .001$; long-delay no-reward effect: $M = -0.43$, 95%
546 CI = [-0.59,-0.25], $p < .001$; Crus II: long-delay reward effect: $M = -0.11$, 95% CI = [-
547 0.25,-0.05], $p = .176$; long-delay no-reward effect: $M = -0.16$, 95% CI = [-0.31,-0.03], $p =$
548 .010).

549 In striatum, the caudate showed a similar effect as the cerebellum
550 (nonparametric bootstrap test: short delays: $M = 0.20$, 95% CI = [0.03, 0.36], $p = .020$;
551 long delays: $M = 0.04$, 95% CI = [-0.11, 0.20], $p = .648$). However, the ventral striatum
552 ROI (NAc) and hippocampus (Hpc) had significant responses at both short and long
553 feedback delays (nonparametric bootstrap test: short delays: NAc: $M = 0.84$, 95% CI =
554 [0.60, 1.08], $p < .001$; Hpc: $M = 0.23$, 95% CI = [0.14, 0.33], $p < .001$; long delays: NAc:
555 $M = 0.64$, 95% CI = [0.45, 0.80], $p < .001$; Hpc: $M = 0.25$, 95% CI = [0.13, 0.36], $p <$
556 .001). Only the cerebellar ROIs exhibited *significantly* stronger responses at short
557 versus long feedback delays (short > long: Crus I: $M = 0.30$, 95% CI = [0.18, 0.44], $p <$

558 .001; Crus II: $M = 0.20$, 95% CI = [0.07, 0.33], $p = .002$; Cd: $M = 0.12$, 95% CI = [-0.01,
559 0.25], $p = .072$; NAc: $M = 0.15$, 95% CI = [-0.01, 0.31], $p = .072$; Hpc: $M = -0.01$, 95% CI
560 = [-0.11, 0.08], $p = .826$). Further, the difference in response to short versus long delay
561 feedback was significantly larger in Crus I than in Cd or Hpc (Crus I: $M = 0.40$; NAc: $M =$
562 0.21 ; Cd: $M = 0.16$; Hpc: $M = -0.02$; Crus I vs NAc: 95% CI = [-0.07, 0.44], $p = .142$;
563 Crus I vs Cd: 95% CI = [0.07, 0.41], $p = .006$; Crus I vs Hpc: 95% CI = [0.15,0.68], $p =$
564 0.002) and in Crus II ($M = 0.27$) than in Hpc (Crus II vs NAc: 95% CI = [-0.2,0.31], $p =$
565 $.614$; Crus II vs Cd: 95% CI = [-0.1, 0.31], $p = .298$; Crus II vs Hpc: 95% CI =
566 [0.05,0.53], $p = 0.016$). Taken together, these results provide evidence for temporally
567 constrained reward processing in the human cerebellum during RL and also show that
568 the delayed feedback did not globally abolish reward signals.

569 *Model-based analyses reveal time-sensitive RPE computations in human cerebellum*

570 We next tested whether the human cerebellum tracked the core teaching signal
571 in RL: reward prediction error (RPE). We leveraged computational modeling to examine
572 RPEs in the cerebellum (**Figure 3a**). To do this, we fit RL models to each participant's
573 behavior to obtain learning and choice parameters for each subject (see *Methods*;
574 **Figure 1c** and **Supplemental Figure 2**). We then used these subject-specific
575 parameters to simulate trial-by-trial RPEs based on a participant's unique sequence of
576 trials and choices. The time course of these computationally inferred RPEs serves as a
577 prediction about activity in regions of the brain that may encode RPE signals. We
578 restricted our main analyses to RPEs on rewarded trials to avoid the strong collinearity
579 with valence signals (see *Methods*; see **Supplemental Figure 3** for RPE results across
580 rewarded and nonrewarded trials).

581 We found robust RPE responses at the boundary of Crus I and Crus II in the
582 cerebellum, in addition to canonical RPE signals in the ventral striatum (**Figure 3b**).
583 Like reward-related activation, RPE responses were temporally constrained, and only
584 detectable on short-delay trials (**Figure 3c** and **Supplemental Figure 3**). Regions
585 within Crus I and II, as well as caudate, showed significant RPE responses at short, but
586 not long delays (**Figure 3d**; nonparametric bootstrap test: short delays: Crus I: $M =$
587 0.65 , $95\% \text{ CI} = [0.47, 0.81]$, $p < .001$; Crus II: $M = 0.45$, $95\% \text{ CI} = [0.28, 0.63]$, $p < .001$;
588 Cd: $M = 0.36$, $95\% \text{ CI} = [0.20, 0.52]$, $p < .001$; long delays: Crus I: $M = -0.30$, $95\% \text{ CI} =$
589 $[-0.46, -0.16]$, $p < .001$; Crus II: $M = 0.01$, $95\% \text{ CI} = [-0.10, 0.12]$, $p = .886$; Cd: $M = -$
590 0.10 , $95\% \text{ CI} = [-0.27, 0.07]$, $p = .268$), while nucleus accumbens and hippocampus
591 displayed robust RPE responses at both short and long delays (short delays: NAc: $M =$
592 0.84 , $95\% \text{ CI} = [0.60, 1.08]$, $p < .001$; Hpc: $M = 0.13$, $95\% \text{ CI} = [0.04, 0.23]$, $p = .002$;
593 long delays: NAc: $M = 0.54$, $95\% \text{ CI} = [0.39, 0.70]$, $p < .001$; Hpc: $M = 0.22$, $95\% \text{ CI} =$
594 $[0.11, 0.33]$, $p < .001$; although stronger at short delays in NAc: short > long: $M = 0.44$,
595 $95\% \text{ CI} = [0.23, 0.65]$, $p < .001$; Foerde & Shohamy, 2011). The difference in RPE
596 encoding for short versus long delay feedback was significantly larger in Crus I than all
597 other ROIs (Crus I: $M = 0.95$; Crus II: $M = 0.44$; NAc: $M = 0.3$; Cd: $M = 0.45$; Hpc: $M = -$
598 0.08 ; Crus I vs NAc: $95\% \text{ CI} = [0.4, 0.92]$, $p < .001$; Crus I vs Cd: $95\% \text{ CI} = [0.26, 0.75]$,
599 $p < .001$; Crus I vs Hpc: $95\% \text{ CI} = [0.78, 1.28]$, $p < .001$) and for Crus II versus Hpc
600 (Crus I vs NAc: $95\% \text{ CI} = [-0.13, 0.43]$, $p = .316$; Crus I vs Cd: $95\% \text{ CI} = [-0.28, 0.26]$, p
601 $= 0.99$; Crus I vs Hpc: $95\% \text{ CI} = [0.29, 0.77]$, $p < .001$). Thus, we found that the human
602 cerebellum encodes prediction errors that are used for learning in a nonmotor learning

603 task, and that these teaching signals may show similar temporal constraints as those
604 observed in sensorimotor learning.

605 RPEs can be signed (i.e., sensitive to valence) or unsigned (i.e., only sensitive to
606 outcome surprise, but not valence). Thus, we used the same approach as above to
607 examine neural correlates of surprise (|RPE|). This analysis, however, did not reveal
608 any significant clusters of activity in the cerebellum, even at a relaxed statistical
609 threshold, suggesting that human cerebellar RPE activity is dominated by a reward-
610 sensitive signal (see *Discussion*).

611 In addition, this model-based analysis framework can be used to examine reward
612 anticipation signals in the brain. Reward anticipation signals can be operationalized as
613 the trial-by-trial Q-value associated with the stimulus that the participant chose. Again,
614 in this exploratory analysis, we identify regions of the brain that have activity that is
615 positively correlated with a computationally inferred value, in this case trial-by-trial Q-
616 values. We did not observe any significant positive activity in cerebellum related to
617 stimulus Q-values, although there was substantial activity in the canonical medial frontal
618 regions that did correlate with stimulus Q-values (**Supplemental Figure 3**; Bartra et al.,
619 2013). We return to this point in the Discussion.

620 *Linking cerebellar RPE activity to behavior*

621 An additional question we asked is whether the apparent cerebellar involvement
622 in RL at short (but not long) feedback delays covaries with behavioral performance in
623 the task. We note that we did not see general performance differences between delay
624 conditions at the group level: On average, participants showed comparable learning and

625 RTs for stimulus pairs associated with short versus long feedback delays (p(choose
626 higher value): $t(31) = 0.51$, 95% CI = [-0.02, 0.04], $p = .616$; RT: $t(31) = 0.03$, 95% CI =
627 [-0.01, 0.01], $p = .976$; **Figure 1d**). However, we did observe individual differences in
628 learning efficacy.

629 To investigate brain-behavior correlations, we compared RPE signals for short
630 versus long delay trials in a whole-brain GLM, and included RL performance in the short
631 delay condition as a participant-wise covariate in the model. In other words, this
632 analysis tests for voxels in the brain where stronger temporally sensitive RPE
633 responses covary with how well a participant performed in the short delay condition.
634 Strikingly, this whole-brain analysis revealed significant brain-behavior correlations only
635 within the cerebellum: The analysis revealed a single significant cluster of activity on the
636 Crus I/II boundary (albeit at a slightly relaxed statistical threshold for the whole-brain
637 case; **Figure 4**; see also **Supplemental Figure 4**). As a control, we also repeated this
638 analysis using performance on the long delay condition, and the difference between
639 performance on the short versus long delay conditions, as covariates, and observed no
640 significant clusters. To visualize this result more clearly, we used a mask of voxels that
641 showed this pattern in cerebellum and plotted activity in this region for each subject
642 against their performance at the short delay condition (**Figure 4c**). Although this
643 analysis is correlational, it suggests that better reinforcement learning (in the short delay
644 condition) was related to stronger temporally-sensitive cerebellar RPEs, thus linking our
645 cerebellar results to behavioral outcomes.

646 *Increased connectivity between cerebellar ROIs and cerebrum during feedback*

647 The cerebellum has bidirectional connections to much of the cerebral RL
648 circuitry, including the basal ganglia and prefrontal cortex (Bostan et al., 2013; Bostan &
649 Strick, 2018). Do cerebellar responses to RL feedback reflect connectivity with a wider
650 cerebellar-striatal-frontal functional circuit? To address this question, we asked which
651 regions of the cerebrum might be functionally coupled with the cerebellum during RL,
652 specifically during feedback processing. We conducted exploratory psycho-
653 physiological interaction analyses (PPI; Di et al., 2021; **Figure 5a**) seeded in our two *a*
654 *priori* anatomical cerebellar ROIs (Crus I and Crus II) to measure if and how functional
655 correlations between the cerebellum and the rest of the brain increase during RL
656 feedback above and beyond other task phases.

657

658 We observed significant activity in the medial prefrontal cortex reflecting robust
659 feedback-sensitive functional connectivity with cognitive regions of the cerebellum
660 during RL, albeit at a slightly relaxed statistical threshold in the case of Crus I (**Figure**
661 **5b & c**). Crus II also showed RL feedback-related functional correlations with lateral
662 PFC regions. Further, at the relaxed statistical threshold, we saw significant connectivity
663 between Crus II and the caudate nucleus (**Figure 5c**), the subcortical region that
664 showed similar temporal sensitivity for RPE responses. These results suggest that
665 nonmotor reward feedback increases functional coupling between the cerebellum and
666 core corticostriatal circuits that support RL.

667 **Discussion**

668 Here, we present evidence of temporally constrained cerebellar involvement in
669 RL in humans. We found that cognitive regions of the human cerebellum (clusters
670 spanning Crus I and II) responded to rewards and encoded reward prediction errors,
671 extending recent work in model organisms (Heffley & Hull, 2019; Kostadinov et al.,
672 2019; Larry et al., 2019; Sendhilnathan et al., 2020; Wagner et al., 2017). These
673 cerebellar RL responses were sensitive to feedback timing, as in motor learning (Gerwig
674 et al., 2008; Ivry & Keele, 1989; Smith, 1968). Further, the degree of time-sensitive RPE
675 encoding covaried with performance on short delay trials, connecting cerebellar RPEs
676 to the efficacy of RL. Finally, functional connectivity analyses revealed communication
677 between the cerebellum and corticostriatal circuitry during feedback (Bostan et al.,
678 2010; Bostan & Strick, 2018; Carta et al., 2019; Hoshi et al., 2005). These results
679 implicate the cerebellum in prediction error-based learning beyond supervised
680 sensorimotor learning, and highlight the importance of examining cerebellar responses
681 in cognitive neuroscience (Wang et al., 2025).

682 We note that our results are not the first to report prediction error signals in the
683 human cerebellum (Lee et al., 2025; O'Doherty et al., 2003) or to suggest that the basal
684 ganglia and cerebellum work collaboratively (Bostan & Strick, 2010). Previous work,
685 however, did not necessarily isolate the signals we see here: First, in previous work,
686 rewards were typically attached to specific motor actions, making it unclear whether
687 cerebellar responses were driven by RL versus sensorimotor learning (Sendhilnathan et
688 al., 2024; Wagner et al., 2017). Similarly, in other studies, reward or punishment
689 feedback had significant sensorimotor components, including shocking of the skin and

690 the ingestion of juice (Maschke et al., 2002; O'Doherty et al., 2003). Such feedback is
691 likely to drive sensorimotor learning processes in the cerebellum, and complicates
692 interpretations of cerebellar prediction error responses.

693 The fact that cerebellar RL signals were temporally sensitive could also explain
694 why similar signals have not been reported consistently in the literature. fMRI studies
695 are typically designed with long delays between stimuli to accommodate the slow
696 hemodynamic response or supra-second TR measurements, which could blunt
697 cerebellar learning signals. Additionally, much human fMRI work does not report what
698 exact regions of the cerebellum are involved. Functional mapping of the cerebellar
699 cortex has revealed a mosaic of functional regions, mirroring the complexity of the
700 cerebral cortex (King et al., 2019; Nettekoven et al., 2024; Saadon-Grosman et al.,
701 2024). These advances make specific localization of cerebellar signals increasingly
702 important, and de-emphasize the functional importance of lobular boundaries. Notably,
703 precision mapping research has characterized multiple functional subregions that are
704 interconnected with distinct cortical and striatal networks (Habas et al., 2009;
705 Nettekoven et al., 2024; Saadon-Grosman et al., 2024). The regions of the cerebellum
706 where we see robust RL signals correspond to social-linguistic-spatial and demand
707 regions (Guell et al., 2018; King et al., 2019; Nettekoven et al., 2024). These regions
708 also exhibit resting state connectivity with default mode areas, and wider frontoparietal
709 and corticostriatal networks (Boonstra, 2025; Dobromyslin et al., 2012; Guell et al.,
710 2018; Habas et al., 2009).

711 Importantly, we were able to draw from the animal literature to make broad *a*
712 *priori* predictions about localization. We found correspondence between RL-sensitive

713 regions reported in research with model organisms and our human participants, despite
714 key differences in experimental design. While model organisms afford exceptional
715 access to recording input and output signals in the cerebellum, one advantage of testing
716 humans is that they can engage in rapid RL over a matter of minutes, respond to verbal
717 instructions, and tolerate higher task variability across trials (e.g., multiple feedback
718 delays). We think this work highlights the preservation of cerebellar function across
719 model organisms and emphasizes the importance of crosstalk between human and
720 animal researchers. This idea is particularly relevant as cerebellar research becomes
721 focused on higher-order cognitive functions (Buckner, 2013; Manto et al., 2024; Strick et
722 al., 2009), and as cognitive neuroscientists increasingly consider cerebellar nonmotor
723 functions.

724 One highlight of this work is that we observed consistent evidence of temporal
725 constraints on cerebellar RL feedback processing; cerebellar encoding of reward and
726 RPE was essentially abolished when feedback was delayed. The idea that the
727 cerebellum is primarily involved in sub-second coordination, associative learning, and
728 timing is well-established in the motor domain (Barri et al., 2022; Gerwig et al., 2008;
729 Ivry & Keele, 1989; Kitazawa et al., 1995; Ohmae & Medina, 2015; Smith, 1968). This
730 preference makes sense for a brain region originally adapted for short-timescale
731 sensorimotor control and prediction (Cisek, 2022). At a mechanistic level, properties of
732 granule cell firing and short-term plasticity at mossy fiber-granule cell synapses have
733 been proposed to support sub-second timing computations characteristic of the
734 cerebellum (Barri et al., 2022; Kennedy et al., 2014; Narain et al., 2018; Yamazaki &
735 Tanaka, 2009). These mechanisms can induce timing-specific activity patterns that are

736 then used by Purkinje cells (the main output neurons of the cerebellum) to refine actions
737 or cognitive computations. There are likely biological limits that constrain what time
738 intervals can be precisely learned by these mechanisms (Raymond & Medina, 2018),
739 providing a mechanistic account for why the cerebellum is attuned to short-timescale
740 feedback.

741 Our model-based analysis approach also allowed for exploratory analyses
742 examining reward anticipation signals. Recent work in animal models has found reward
743 anticipation signals during RL in analogous regions (Wagner et al., 2017; Larry et al.,
744 2019; Kostadinov et al., 2019; Heffley & Hull, 2019). For example, Larry et al. (2019)
745 observed climbing fiber responses that scaled with expected reward during the *cue*
746 phase of a RL task (as in classic Temporal-Difference learning; Sutton & Barto, 1998),
747 echoing observations in the domain of eyeblink conditioning (Ohmae et al., 2015).
748 Similarly, Wagner et al. (2017) reported granule cell activity ramping toward an
749 expected reward. In contrast, we did not see significant positive cerebellar activity
750 correlating with trialwise Q-values (**Supplemental Figure 3**). Why the discrepancy
751 between our results and recent work in animal models?

752 The most likely explanation is the major differences in methodological
753 approaches between human fMRI study and electrophysiological approaches. BOLD
754 signals in cerebellum primarily track activity in the mossy fiber-granule cell input
755 pathway to the cerebellum (Shahshahani et al., 2024). Thus, climbing fiber signals at
756 choice may be a relatively weak contribution to the BOLD signal versus combined
757 climbing fiber and mossy fiber-granule cell activity during feedback. As for ramping
758 signals (Wagner et al., 2017), these may be hard to separate from feedback-related

759 responses given the low temporal resolution of fMRI. Finally, while model-based
760 analyses are extremely useful for making predictions about RPE activity, it is important
761 to remember that these RPE timecourses are inferred from a necessarily simplified
762 model of RL and model fit may vary considerably across participants.

763 Our connectivity analyses implicate communication between cognitive regions of
764 the cerebellum and neocortical and subcortical regions during RL feedback processing.
765 Some regions of medial PFC also emerged in our reward processing and RPE
766 analyses, perhaps suggesting that co-fluctuations between the cerebellum and these
767 regions are driven by the receipt of rewards. Lateral PFC, in contrast, was not a reward-
768 sensitive region in other analyses. Communication between cerebellum and lateral PFC
769 could reflect general feedback processing, perhaps updating predictions based on new
770 feedback. One caveat is that PPI cannot distinguish between correlations in activity due
771 to functional connectivity versus high correlations in activity driven by alternative
772 sources of shared input (Friston et al., 1997; Sanchez-Romero et al., 2019). The
773 existence of anatomical connections between cerebellum and prefrontal regions via the
774 dentate nucleus and thalamus (Kelly & Strick, 2003) are consistent with a functional
775 coupling explanation, however future work with causal manipulations are necessary to
776 resolve this issue.

777 Although we are primarily measuring cerebellar input, communication likely
778 involves bidirectional connections between the cerebellum and frontal and subcortical
779 RL regions (Boonstra, 2025; Bostan & Strick, 2010, 2018; Hoshi et al., 2005; Saadon-
780 Grosman et al., 2024; Wagner & Luo, 2020). A recent fMRI paper demonstrated how
781 cerebellar-striatal connectivity might support reward-based motor learning (Lee et al.,

782 2025); in contrast to our work, they found that cerebellar activity primarily tracked
783 surprise (i.e., unsigned prediction error magnitude). Indeed, we did not find significant
784 activation in the cerebellum tracking surprise. This discrepancy is likely due to
785 significant task differences, where cerebellar signals in Lee and colleagues (2025) were
786 associated with successful versus unsuccessful outcomes of a motor task, not a
787 nonmotor RL task as presented here.

788 Overall, our results provide evidence of temporally-constrained, behaviorally-
789 relevant RL signals in the human cerebellum. RPE and reward-related signals were
790 prominent in cognitive regions of the cerebellum, corresponding with recent work in
791 animal models. Connectivity results demonstrated functional correlations between
792 functional subregions spanning Crus I and II and regions of the medial and lateral
793 frontal cortex and caudate nucleus during RL. This work extends beyond the well-
794 studied role of the cerebellum in prediction-error based supervised motor learning
795 (Albus, 1971; Hull, 2020b; Marr, 1969; Raymond & Medina, 2018; Wolpert et al., 1998),
796 and contributes to growing evidence that the human cerebellum may support prediction-
797 error based learning across multiple domains.

798 **References**

- 799 Albus, J. S. (1971). A theory of cerebellar function. *Mathematical Biosciences*, 10(1–2),
800 25–61. [https://doi.org/10.1016/0025-5564\(71\)90051-4](https://doi.org/10.1016/0025-5564(71)90051-4)
- 801 Avants, B. B., Epstein, C. L., Grossman, M., & Gee, J. C. (2008). Symmetric
802 diffeomorphic image registration with cross-correlation: Evaluating automated
803 labeling of elderly and neurodegenerative brain. *Medical Image Analysis, Special
804 Issue on The Third International Workshop on Biomedical Image Registration –
805 WBIR 2006*, 12(1), 26–41. <https://doi.org/10.1016/j.media.2007.06.004>
- 806 Avraham, G., Taylor, J. A., Breska, A., Ivry, R. B., & McDougle, S. D. (2022). Contextual
807 effects in sensorimotor adaptation adhere to associative learning rules. *eLife*, 11,
808 e75801. <https://doi.org/10.7554/eLife.75801>
- 809 Barri, A., Wiechert, M. T., Jazayeri, M., & DiGregorio, D. A. (2022). Synaptic basis of a
810 sub-second representation of time in a neural circuit model. *Nature
811 Communications*, 13(1), 7902. <https://doi.org/10.1038/s41467-022-35395-y>
- 812 Behzadi, Y., Restom, K., Liao, J., & Liu, T. T. (2007). A component based noise
813 correction method (CompCor) for BOLD and perfusion based fMRI. *NeuroImage*,
814 37(1), 90–101. <https://doi.org/10.1016/j.neuroimage.2007.04.042>
- 815 Boonstra, J. T. (2025). The cerebellar connectome. *Behavioural Brain Research*, 482,
816 115457. <https://doi.org/10.1016/j.bbr.2025.115457>
- 817 Boorman, E. D., Behrens, T. E., & Rushworth, M. F. (2011). Counterfactual Choice and
818 Learning in a Neural Network Centered on Human Lateral Frontopolar Cortex.
819 *PLOS Biology*, 9(6), e1001093. <https://doi.org/10.1371/journal.pbio.1001093>

820 Bostan, A. C., Dum, R. P., & Strick, P. L. (2010). The basal ganglia communicate with
821 the cerebellum. *Proceedings of the National Academy of Sciences*, *107*(18),
822 8452–8456. <https://doi.org/10.1073/pnas.1000496107>

823 Bostan, A. C., Dum, R. P., & Strick, P. L. (2013). Cerebellar networks with the cerebral
824 cortex and basal ganglia. *Trends in Cognitive Sciences*, *17*(5), 241–254.
825 <https://doi.org/10.1016/j.tics.2013.03.003>

826 Bostan, A. C., & Strick, P. L. (2010). The Cerebellum and Basal Ganglia are
827 Interconnected. *Neuropsychology Review*, *20*(3), 261–270.
828 <https://doi.org/10.1007/s11065-010-9143-9>

829 Bostan, A. C., & Strick, P. L. (2018). The basal ganglia and the cerebellum: Nodes in an
830 integrated network. *Nature Reviews Neuroscience*, *19*(6), 338–350.
831 <https://doi.org/10.1038/s41583-018-0002-7>

832 Brudner, S. N., Kethidi, N., Graeupner, D., Ivry, R. B., & Taylor, J. A. (2016). Delayed
833 feedback during sensorimotor learning selectively disrupts adaptation but not
834 strategy use. *Journal of Neurophysiology*, *115*(3), 1499–1511.
835 <https://doi.org/10.1152/jn.00066.2015>

836 Buckner, R. L. (2013). The Cerebellum and Cognitive Function: 25 Years of Insight from
837 Anatomy and Neuroimaging. *Neuron*, *80*(3), 807–815.
838 <https://doi.org/10.1016/j.neuron.2013.10.044>

839 Buckner, R. L., Krienen, F. M., Castellanos, A., Diaz, J. C., & Yeo, B. T. T. (2011). The
840 organization of the human cerebellum estimated by intrinsic functional

841 connectivity. *Journal of Neurophysiology*, 106(5), 2322–2345.
842 <https://doi.org/10.1152/jn.00339.2011>

843 Buhusi, C. V., & Meck, W. H. (2005). What makes us tick? Functional and neural
844 mechanisms of interval timing. *Nature Reviews Neuroscience*, 6(10), 755–765.
845 <https://doi.org/10.1038/nrn1764>

846 Butcher, P. A., Ivry, R. B., Kuo, S.-H., Rydz, D., Krakauer, J. W., & Taylor, J. A. (2017).
847 The cerebellum does more than sensory prediction error-based learning in
848 sensorimotor adaptation tasks. *Journal of Neurophysiology*, 118(3), 1622–1636.
849 <https://doi.org/10.1152/jn.00451.2017>

850 Carta, I., Chen, C. H., Schott, A. L., Dorizan, S., & Khodakhah, K. (2019). Cerebellar
851 modulation of the reward circuitry and social behavior. *Science*, 363(6424).
852 <https://doi.org/10.1126/science.aav0581>

853 Cheng, D. T., Disterhoft, J. F., Power, J. M., Ellis, D. A., & Desmond, J. E. (2008).
854 Neural substrates underlying human delay and trace eyeblink conditioning.
855 *Proceedings of the National Academy of Sciences*, 105(23), 8108–8113.
856 <https://doi.org/10.1073/pnas.0800374105>

857 Chettih, S. N., McDougle, S. D., Ruffolo, L. I., & Medina, J. F. (2011). Adaptive Timing
858 of Motor Output in the Mouse: The Role of Movement Oscillations in Eyelid
859 Conditioning. *Frontiers in Integrative Neuroscience*, 5.
860 <https://doi.org/10.3389/fnint.2011.00072>

861 Cisek, P. (2022). Evolution of behavioural control from chordates to primates.
862 *Philosophical Transactions of the Royal Society B: Biological Sciences*,
863 377(1844), 20200522. <https://doi.org/10.1098/rstb.2020.0522>

864 Cohen, J. D., Daw, N., Engelhardt, B., Hasson, U., Li, K., Niv, Y., Norman, K. A., Pillow,
865 J., Ramadge, P. J., Turk-Browne, N. B., & Willke, T. L. (2017). Computational
866 approaches to fMRI analysis. *Nature Neuroscience*, 20(3), 304–313.
867 <https://doi.org/10.1038/nn.4499>

868 Dale, A. M., Fischl, B., & Sereno, M. I. (1999). Cortical Surface-Based Analysis: I.
869 Segmentation and Surface Reconstruction. *NeuroImage*, 9(2), 179–194.
870 <https://doi.org/10.1006/nimg.1998.0395>

871 Di, X., Zhang, Z., & Biswal, B. B. (2021). Understanding psychophysiological interaction
872 and its relations to beta series correlation. *Brain Imaging and Behavior*, 15(2),
873 958–973. <https://doi.org/10.1007/s11682-020-00304-8>

874 Diedrichsen, J. (2006). *A spatially unbiased atlas template of the human cerebellum*.

875 Diedrichsen, J., Balsters, J. H., Flavell, J., Cussans, E., & Ramnani, N. (2009). *A*
876 *probabilistic MR atlas of the human cerebellum*.

877 Diedrichsen, J., King, M., Hernandez-Castillo, C., Sereno, M., & Ivry, R. B. (2019).
878 Universal Transform or Multiple Functionality? Understanding the Contribution of
879 the Human Cerebellum across Task Domains. *Neuron*, 102(5), 918–928.
880 <https://doi.org/10.1016/j.neuron.2019.04.021>

881 Diedrichsen, J., & McDougle, S. D. (2026). How does the cerebellum contribute to
882 cognitive functions? *PLOS Biology*, 24(3), e3003688.
883 <https://doi.org/10.1371/journal.pbio.3003688>

884 Diedrichsen, J., Verstynen, T., Schlerf, J., & Wiestler, T. (2010). Advances in functional
885 imaging of the human cerebellum: *Current Opinion in Neurology*, 23, 382–387.
886 <https://doi.org/10.1097/WCO.0b013e32833be837>

887 Diedrichsen, J., & Zotow, E. (2015). Surface-Based Display of Volume-Averaged
888 Cerebellar Imaging Data. *PLOS ONE*, 10(7), e0133402.
889 <https://doi.org/10.1371/journal.pone.0133402>

890 Dobromyslin, V. I., Salat, D. H., Fortier, C. B., Leritz, E. C., Beckmann, C. F., Milberg,
891 W. P., & McGlinchey, R. E. (2012). Distinct functional networks within the
892 cerebellum and their relation to cortical systems assessed with independent
893 component analysis. *NeuroImage*, 60(4), 2073–2085.
894 <https://doi.org/10.1016/j.neuroimage.2012.01.139>

895 Drepper, J., Timmann, D., Kolb, F. P., & Diener, H. C. (1999). Non-motor associative
896 learning in patients with isolated degenerative cerebellar disease. *Brain*, 122(1),
897 87–97. <https://doi.org/10.1093/brain/122.1.87>

898 Eli Billauer. (2009). *Peakdet* (Version 3.4.05) [MATLAB].

899 Esteban, O., Markiewicz, C. J., Blair, R. W., Moodie, C. A., Isik, A. I., Erramuzpe, A.,
900 Kent, J. D., Goncalves, M., DuPre, E., Snyder, M., Oya, H., Ghosh, S. S., Wright,
901 J., Durnez, J., Poldrack, R. A., & Gorgolewski, K. J. (2019). fMRIPrep: A robust

902 preprocessing pipeline for functional MRI. *Nature Methods*, 16(1), 111–116.
903 <https://doi.org/10.1038/s41592-018-0235-4>

904 Esteban, O., Ross, B., Markiewicz, C. J., Berleant, S. L., Moodie, C., Ma, F., & Isik, A. I.
905 (2018). *fMRIPrep 23.2.1*. [Computer software].
906 <https://doi.org/10.5281/zenodo.852659>

907 Foerde, K., & Shohamy, D. (2011). The role of the basal ganglia in learning and
908 memory: Insight from Parkinson's disease. *Neurobiology of Learning and*
909 *Memory*, 96(4), 624–636. <https://doi.org/10.1016/j.nlm.2011.08.006>

910 Frank, M. J., Moustafa, A. A., Haughey, H. M., Curran, T., & Hutchison, K. E. (2007).
911 Genetic triple dissociation reveals multiple roles for dopamine in reinforcement
912 learning. *Proceedings of the National Academy of Sciences*, 104(41), 16311–
913 16316. <https://doi.org/10.1073/pnas.0706111104>

914 Friston, K. J., Buechel, C., Fink, G. R., Morris, J., Rolls, E., & Dolan, R. J. (1997).
915 Psychophysiological and Modulatory Interactions in Neuroimaging. *NeuroImage*,
916 6(3), 218–229. <https://doi.org/10.1006/nimg.1997.0291>

917 Garrison, J., Erdeniz, B., & Done, J. (2013). Prediction error in reinforcement learning: A
918 meta-analysis of neuroimaging studies. *Neuroscience and Biobehavioral*
919 *Reviews*, 37(7), 1297–1310. <https://doi.org/10.1016/j.neubiorev.2013.03.023>

920 Gerwig, M., Eßer, A. C., Guberina, H., Frings, M., Kolb, F. P., Forsting, M., Aurich, V.,
921 Beck, A., & Timmann, D. (2008). Trace eyeblink conditioning in patients with
922 cerebellar degeneration: Comparison of short and long trace intervals.

923 *Experimental Brain Research*, 187(1), 85–96. <https://doi.org/10.1007/s00221->
924 008-1283-2

925 Gitelman, D. R., Penny, W. D., Ashburner, J., & Friston, K. J. (2003). Modeling regional
926 and psychophysiologic interactions in fMRI: The importance of hemodynamic
927 deconvolution. *NeuroImage*, 19(1), 200–207. <https://doi.org/10.1016/S1053->
928 8119(03)00058-2

929 Gorgolewski, K., Burns, C. D., Madison, C., Clark, D., Halchenko, Y. O., Waskom, M. L.,
930 & Ghosh, S. S. (2011). Nipype: A Flexible, Lightweight and Extensible
931 Neuroimaging Data Processing Framework in Python. *Frontiers in*
932 *Neuroinformatics*, 5. <https://doi.org/10.3389/fninf.2011.00013>

933 Greve, D. N., & Fischl, B. (2009). Accurate and robust brain image alignment using
934 boundary-based registration. *NeuroImage*, 48(1), 63–72.
935 <https://doi.org/10.1016/j.neuroimage.2009.06.060>

936 Guell, X., Schmahmann, J. D., Gabrieli, J. D., & Ghosh, S. S. (2018). Functional
937 gradients of the cerebellum. *eLife*, 7, e36652. <https://doi.org/10.7554/eLife.36652>

938 Habas, C., Kamdar, N., Nguyen, D., Prater, K., Beckmann, C. F., Menon, V., & Greicius,
939 M. D. (2009). Distinct Cerebellar Contributions to Intrinsic Connectivity Networks.
940 *Journal of Neuroscience*, 29(26), 8586–8594.
941 <https://doi.org/10.1523/JNEUROSCI.1868-09.2009>

942 Heffley, W., & Hull, C. (2019). Classical conditioning drives learned reward prediction
943 signals in climbing fibers across the lateral cerebellum. *eLife*, 8, 8–10.
944 <https://doi.org/10.7554/eLife.46764>

945 Heffley, W., Song, E. Y., Xu, Z., Taylor, B. N., Hughes, M. A., McKinney, A., Joshua, M.,
946 & Hull, C. (2018). Coordinated cerebellar climbing fiber activity signals learned
947 sensorimotor predictions. *Nature Neuroscience*, 21(10), 1431–1441.
948 <https://doi.org/10.1038/s41593-018-0228-8>

949 Hoshi, E., Tremblay, L., Féger, J., Carras, P. L., & Strick, P. L. (2005). The cerebellum
950 communicates with the basal ganglia. *Nature Neuroscience*, 8(11), 1491–1493.
951 <https://doi.org/10.1038/nn1544>

952 Hull, C. (2020a). Prediction signals in the cerebellum: Beyond supervised motor
953 learning. *eLife*, 9, e54073. <https://doi.org/10.7554/eLife.54073>

954 Hull, C. (2020b). Prediction signals in the cerebellum: Beyond supervised motor
955 learning. *eLife*, 9, e54073. <https://doi.org/10.7554/eLife.54073>

956 Huvermann, D. M., Berlijn, A. M., Thieme, A., Erdlenbruch, F., Groiss, S. J., Deistung,
957 A., Mittelstaedt, M., Wondzinski, E., Sievers, H., Frank, B., Göricke, S. L., Gliem,
958 M., Köhrmann, M., Siebler, M., Schnitzler, A., Bellebaum, C., Minnerop, M.,
959 Timmann, D., & Peterburs, J. (2025). The cerebellum contributes to prediction
960 error coding in reinforcement learning in humans. *Journal of Neuroscience*.
961 <https://doi.org/10.1523/JNEUROSCI.1972-24.2025>

962 Iadecola, C., Yang, G., Ebner, T. J., & Chen, G. (1997). Local and Propagated Vascular
963 Responses Evoked by Focal Synaptic Activity in Cerebellar Cortex. *Journal of*
964 *Neurophysiology*, 78(2), 651–659. <https://doi.org/10.1152/jn.1997.78.2.651>

965 Ito, M. (2008). Control of mental activities by internal models in the cerebellum. *Nature*
966 *Reviews Neuroscience*, 9(4), 304–313. <https://doi.org/10.1038/nrn2332>

967 Ivry, R. B., & Keele, S. W. (1989). Timing Functions of The Cerebellum. *Journal of*
968 *Cognitive Neuroscience*, 1(2), 136–152.
969 <https://doi.org/10.1162/jocn.1989.1.2.136>

970 Jenkinson, M., Bannister, P., Brady, M., & Smith, S. (2002). Improved Optimization for
971 the Robust and Accurate Linear Registration and Motion Correction of Brain
972 Images. *NeuroImage*, 17(2), 825–841. <https://doi.org/10.1006/nimg.2002.1132>

973 Kelly, R. M., & Strick, P. L. (2003). Cerebellar Loops with Motor Cortex and Prefrontal
974 Cortex of a Nonhuman Primate. *The Journal of Neuroscience*, 23(23), 8432–
975 8444. <https://doi.org/10.1523/JNEUROSCI.23-23-08432.2003>

976 Kennedy, A., Wayne, G., Kaifosh, P., Alviña, K., Abbott, L. F., & Sawtell, N. B. (2014). A
977 temporal basis for predicting the sensory consequences of motor commands in
978 an electric fish. *Nature Neuroscience*, 17(3), 416–422.
979 <https://doi.org/10.1038/nn.3650>

980 King, M., Hernandez-Castillo, C. R., Poldrack, R. A., Ivry, R. B., & Diedrichsen, J.
981 (2019). Functional boundaries in the human cerebellum revealed by a multi-
982 domain task battery. *Nature Neuroscience*, 22(8), 1371–1378.
983 <https://doi.org/10.1038/s41593-019-0436-x>

984 King, M., Shahshahani, L., Ivry, R. B., & Diedrichsen, J. (2023). A task-general
985 connectivity model reveals variation in convergence of cortical inputs to
986 functional regions of the cerebellum. *eLife*, 12, e81511.
987 <https://doi.org/10.7554/eLife.81511>

988 Kitazawa, S., Kohno, T., & Uka, T. (1995). Effects of delayed visual information on the
989 rate and amount of prism adaptation in the human. *The Journal of Neuroscience*,
990 15(11), 7644–7652. <https://doi.org/10.1523/JNEUROSCI.15-11-07644.1995>

991 Klein, A., Ghosh, S. S., Bao, F. S., Giard, J., Häme, Y., Stavsky, E., Lee, N., Rossa, B.,
992 Reuter, M., Neto, E. C., & Keshavan, A. (2017). Mindboggling morphometry of
993 human brains. *PLOS Computational Biology*, 13(2), e1005350.
994 <https://doi.org/10.1371/journal.pcbi.1005350>

995 Kostadinov, D., Beau, M., Pozo, M. B., & Häusser, M. (2019). Predictive and reactive
996 reward signals conveyed by climbing fiber inputs to cerebellar Purkinje cells.
997 *Nature Neuroscience*, 22(6), 950–962. [https://doi.org/10.1038/s41593-019-0381-](https://doi.org/10.1038/s41593-019-0381-8)
998 8

999 Kostadinov, D., & Häusser, M. (2022). Reward signals in the cerebellum: Origins,
1000 targets, and functional implications. *Neuron*, 110(8), 1290–1303.
1001 <https://doi.org/10.1016/j.neuron.2022.02.015>

1002 Kruithof, E. S., Klaus, J., & Schutter, D. J. L. G. (2023). The human cerebellum in
1003 reward anticipation and outcome processing: An activation likelihood estimation
1004 meta-analysis. *Neuroscience & Biobehavioral Reviews*, 149, 105171.
1005 <https://doi.org/10.1016/j.neubiorev.2023.105171>

1006 Krzysztof J. Gorgolewski, Oscar Esteban, Christopher J. Markiewicz, Erik Ziegler,
1007 David Gage Ellis, Michael Philipp Notter, & Dorota Jarecka. (2018). *Nipype*
1008 [Computer software]. <https://doi.org/10.5281/zenodo.596855>

1009 Larry, N., Yarkoni, M., Lixenberg, A., & Joshua, M. (2019). Cerebellar climbing fibers
1010 encode expected reward size. *eLife*, 8, 1–16. <https://doi.org/10.7554/eLife.46870>

1011 Lee, J. L., Casamento-Moran, A., Bastian, A. J., Cullen, K. E., & Chib, V. S. (2025).
1012 Striatal and cerebellar interactions during reward-based motor performance.
1013 *Proceedings of the National Academy of Sciences*, 122(32), e2503373122.
1014 <https://doi.org/10.1073/pnas.2503373122>

1015 Leiner, H. C., Leiner, A. L., & Dow, R. S. (1986). Does the cerebellum contribute to
1016 mental skills? *Behavioral Neuroscience*, 100(4), 443–454.
1017 <https://doi.org/10.1037/0735-7044.100.4.443>

1018 Leong, Y. C., Radulescu, A., Daniel, R., DeWoskin, V., & Niv, Y. (2017). Dynamic
1019 Interaction between Reinforcement Learning and Attention in Multidimensional
1020 Environments. *Neuron*, 93(2), 451–463.
1021 <https://doi.org/10.1016/j.neuron.2016.12.040>

1022 Manto, M., Adamaszek, M., Apps, R., Carlson, E., Guarque-Chabrera, J., Heleven, E.,
1023 Kakei, S., Khodakhah, K., Kuo, S.-H., Lin, C.-Y. R., Joshua, M., Miquel, M.,
1024 Mitoma, H., Larry, N., Péron, J. A., Pickford, J., Schutter, D. J. L. G., Singh, M.
1025 K., Tan, T., ... Yamashiro, K. (2024). Consensus Paper: Cerebellum and
1026 Reward. *The Cerebellum*, 23(5), 2169–2192. [https://doi.org/10.1007/s12311-024-](https://doi.org/10.1007/s12311-024-01702-0)
1027 [01702-0](https://doi.org/10.1007/s12311-024-01702-0)

1028 Marr, D. (1969). A theory of cerebellar cortex. *The Journal of Physiology*, 202(2), 437–
1029 470. <https://doi.org/10.1113/jphysiol.1969.sp008820>

1030 Maschke, M., Schugens, M., Kindsvater, K., Drepper, J., Kolb, F. P., Diener, H.-C.,
1031 Daum, I., & Timmann, D. (2002). Fear conditioned changes of heart rate in
1032 patients with medial cerebellar lesions. *Journal of Neurology, Neurosurgery and*
1033 *Psychiatry*, 72(1), 116–118.

1034 McDougle, S. D., Boggess, M. J., Crossley, M. J., Parvin, D., Ivry, R. B., & Taylor, J. A.
1035 (2016). Credit assignment in movement-dependent reinforcement learning.
1036 *Proceedings of the National Academy of Sciences of the United States of*
1037 *America*, 113(24), 6797–6802. <https://doi.org/10.1073/pnas.1523669113>

1038 McDougle, S. D., Tsay, J. S., Pitt, B., King, M., Saban, W., Taylor, J. A., & Ivry, R. B.
1039 (2022). Continuous manipulation of mental representations is compromised in
1040 cerebellar degeneration. *Brain*, awac072. <https://doi.org/10.1093/brain/awac072>

1041 Middleton, F. A., & Strick, P. L. (1994). Anatomical Evidence for Cerebellar and Basal
1042 Ganglia Involvement in Higher Cognitive Function. *Science*, 266(5184), 458–461.
1043 <https://doi.org/10.1126/science.7939688>

1044 Narain, D., Remington, E. D., Zeeuw, C. I. D., & Jazayeri, M. (2018). A cerebellar
1045 mechanism for learning prior distributions of time intervals. *Nature*
1046 *Communications*, 9(1), 469. <https://doi.org/10.1038/s41467-017-02516-x>

1047 Nettekoven, C., Zhi, D., Shahshahani, L., Pinho, A. L., Saadon-Grosman, N., Buckner,
1048 R. L., & Diedrichsen, J. (2024). A hierarchical atlas of the human cerebellum for
1049 functional precision mapping. *Nature Communications*, 15(1), 8376.
1050 <https://doi.org/10.1038/s41467-024-52371-w>

1051 Nicholas, J., Amlang, C., Lin, C.-Y. R., Montaser-Kouhsari, L., Desai, N., Pan, M.-K.,
1052 Kuo, S.-H., & Shohamy, D. (2023). The Role of the Cerebellum in Learning to
1053 Predict Reward: Evidence from Cerebellar Ataxia. *The Cerebellum*, 23(4), 1355–
1054 1368. <https://doi.org/10.1007/s12311-023-01633-2>

1055 O’Doherty, J. P., Dayan, P., Friston, K., Critchley, H., & Dolan, R. J. (2003). Temporal
1056 difference models and reward-related learning in the human brain. *Neuron*, 38(2),
1057 329–337. [https://doi.org/10.1016/S0896-6273\(03\)00169-7](https://doi.org/10.1016/S0896-6273(03)00169-7)

1058 Ohmae, S., & Medina, J. F. (2015). Climbing fibers encode a temporal-difference
1059 prediction error during cerebellar learning in mice. *Nature Neuroscience*, 18(12),
1060 1798–1803. <https://doi.org/10.1038/nn.4167>

1061 Patriat, R., Reynolds, R. C., & Birn, R. M. (2017). An improved model of motion-related
1062 signal changes in fMRI. *NeuroImage*, 144, 74–82.
1063 <https://doi.org/10.1016/j.neuroimage.2016.08.051>

1064 Power, J. D., Mitra, A., Laumann, T. O., Snyder, A. Z., Schlaggar, B. L., & Petersen, S.
1065 E. (2014). Methods to detect, characterize, and remove motion artifact in resting
1066 state fMRI. *NeuroImage*, 84, 320–341.
1067 <https://doi.org/10.1016/j.neuroimage.2013.08.048>

1068 Raymond, J. L., & Medina, J. F. (2018). Computational principles of supervised learning
1069 in the cerebellum. *Annual Review of Neuroscience*, 41, 233–253.
1070 <https://doi.org/10.1146/annurev-neuro-080317-061948>

1071 Saadon-Grosman, N., Du, J., Kosakowski, H. L., Angeli, P. A., DiNicola, L. M., Eldaief,
1072 M. C., & Buckner, R. L. (2024). Within-individual organization of the human

1073 cognitive cerebellum: Evidence for closely juxtaposed, functionally specialized
1074 regions. *Science Advances*, 10(45), eadq4037.
1075 <https://doi.org/10.1126/sciadv.adq4037>

1076 Sanchez-Romero, R., Ramsey, J. D., Zhang, K., Glymour, M. R. K., Huang, B., &
1077 Glymour, C. (2019). Estimating feedforward and feedback effective connections
1078 from fMRI time series: Assessments of statistical methods. *Network
1079 Neuroscience*, 3(2), 274–306. https://doi.org/10.1162/netn_a_00061

1080 Satterthwaite, T. D., Elliott, M. A., Gerraty, R. T., Ruparel, K., Loughhead, J., Calkins, M.
1081 E., Eickhoff, S. B., Hakonarson, H., Gur, R. C., Gur, R. E., & Wolf, D. H. (2013).
1082 An improved framework for confound regression and filtering for control of motion
1083 artifact in the preprocessing of resting-state functional connectivity data.
1084 *NeuroImage*, 64, 240–256. <https://doi.org/10.1016/j.neuroimage.2012.08.052>

1085 Schlerf, J., Ivry, R. B., & Diedrichsen, J. (2012). Encoding of Sensory Prediction Errors
1086 in the Human Cerebellum. *Journal of Neuroscience*, 32(14), 4913–4922.
1087 <https://doi.org/10.1523/JNEUROSCI.4504-11.2012>

1088 Schmahmann, J. D. (2019). The cerebellum and cognition. *Neuroscience Letters*,
1089 688(April 2018), 62–75. <https://doi.org/10.1016/j.neulet.2018.07.005>

1090 Schmahmann, J. D., & Sherman, J. C. (1998). The cerebellar cognitive affective
1091 syndrome. *Brain*, 121(4), 561–579. <https://doi.org/10.1093/brain/121.4.561>

1092 Sendhilnathan, N., Bostan, A. C., Strick, P. L., & Goldberg, M. E. (2024). A cerebro-
1093 cerebellar network for learning visuomotor associations. *Nature Communications*,
1094 15(1), 2519. <https://doi.org/10.1038/s41467-024-46281-0>

1095 Sendhilnathan, N., Ipata, A. E., & Goldberg, M. E. (2020). Neural Correlates of
1096 Reinforcement Learning in Mid-lateral Cerebellum. *Neuron*, *106*(1), 188-198.e5.
1097 <https://doi.org/10.1016/j.neuron.2019.12.032>

1098 Seymour, B., O'Doherty, J. P., Dayan, P., Koltzenburg, M., Jones, A. K., Dolan, R. J.,
1099 Friston, K. J., & Frackowiak, R. S. (2004). Temporal difference models describe
1100 higher-order learning in humans. *Nature*, *429*(6992), 664–667.
1101 <https://doi.org/10.1038/nature02581>

1102 Shahshahani, L., King, M., Nettekoven, C., Ivry, R. B., & Diedrichsen, J. (2024).
1103 Selective recruitment of the cerebellum evidenced by task-dependent gating of
1104 inputs. *eLife*, *13*, RP96386. <https://doi.org/10.7554/eLife.96386>

1105 Smith, M. C. (1968). CS-US interval and US intensity in classical conditioning of the
1106 rabbit's nictitating membrane response. *Journal of Comparative and*
1107 *Physiological Psychology*, *66*(3, Pt.1), 679–687.
1108 <https://doi.org/10.1037/h0026550>

1109 Sokolov, A. A., Miall, R. C., & Ivry, R. B. (2017). The Cerebellum: Adaptive Prediction
1110 for Movement and Cognition. *Trends in Cognitive Sciences*, *21*(5), 313–332.
1111 <https://doi.org/10.1016/j.tics.2017.02.005>

1112 Stoodley, C. J. (2016). The cerebellum and neurodevelopmental disorders. *The*
1113 *Cerebellum*, *15*(1), 34–37. <https://doi.org/10.1007/s12311-015-0715-3>

1114 Stoodley, C. J., Valera, E. M., & Schmahmann, J. D. (2012). Functional topography of
1115 the cerebellum for motor and cognitive tasks: An fMRI study. *NeuroImage*, *59*(2),
1116 1560–1570. <https://doi.org/10.1016/j.neuroimage.2011.08.065>

- 1117 Strick, P. L., Dum, R. P., & Fiez, J. A. (2009). Cerebellum and Nonmotor Function.
1118 *Annual Review of Neuroscience*, 32(1), 413–434.
1119 <https://doi.org/10.1146/annurev.neuro.31.060407.125606>
- 1120 Strierner, C. L., Chouinard, P. A., Goodale, M. A., & de Ribaupierre, S. (2015).
1121 Overlapping neural circuits for visual attention and eye movements in the human
1122 cerebellum. *Neuropsychologia*, 69, 9–21.
1123 <https://doi.org/10.1016/j.neuropsychologia.2015.01.024>
- 1124 Sutton, R. S., & Barto, A. G. (1998). *Introduction to reinforcement learning*.
- 1125 Timmann, D., Drepper, J., Frings, M., Maschke, M., Richter, S., Gerwig, M., & Kolb, F.
1126 P. (2010). The human cerebellum contributes to motor, emotional and cognitive
1127 associative learning. A review. *Cortex*, 46(7), 845–857.
1128 <https://doi.org/10.1016/j.cortex.2009.06.009>
- 1129 Trach, J. E., deBettencourt, M. T., Radulescu, A., & McDougle, S. D. (2025). Rewards
1130 transiently and automatically enhance sustained attention. *Journal of*
1131 *Experimental Psychology: General*, 154(4), 1063–1079.
1132 <https://doi.org/10.1037/xge0001727>
- 1133 Tustison, N. J., Avants, B. B., Cook, P. A., Zheng, Y., Egan, A., Yushkevich, P. A., &
1134 Gee, J. C. (2010). N4ITK: Improved N3 Bias Correction. *IEEE Transactions on*
1135 *Medical Imaging*, 29(6), 1310–1320. <https://doi.org/10.1109/TMI.2010.2046908>
- 1136 Van Overwalle, F., Baetens, K., Mariën, P., & Vandekerckhove, M. (2014). Social
1137 cognition and the cerebellum: A meta-analysis of over 350 fMRI studies.
1138 *NeuroImage*, 86, 554–572. <https://doi.org/10.1016/j.neuroimage.2013.09.033>

- 1139 Van Overwalle, F., Manto, M., Cattaneo, Z., Clausi, S., Ferrari, C., Gabrieli, J. D. E.,
1140 Guell, X., Heleven, E., Lupo, M., Ma, Q., Michelutti, M., Olivito, G., Pu, M., Rice,
1141 L. C., Schmahmann, J. D., Siciliano, L., Sokolov, A. A., Stoodley, C. J., van Dun,
1142 K., ... Leggio, M. (2020). Consensus Paper: Cerebellum and Social Cognition.
1143 *The Cerebellum*, 19(6), 833–868. <https://doi.org/10.1007/s12311-020-01155-1>
- 1144 Wagner, M. J., Kim, T. H., Savall, J., Schnitzer, M. J., & Luo, L. (2017). Cerebellar
1145 granule cells encode the expectation of reward. *Nature*, 544(7648), 96–100.
1146 <https://doi.org/10.1038/nature21726>
- 1147 Wagner, M. J., & Luo, L. (2020). Neocortex–Cerebellum Circuits for Cognitive
1148 Processing. *Trends in Neurosciences*, 43(1), 42–54.
1149 <https://doi.org/10.1016/j.tins.2019.11.002>
- 1150 Wang, B., LeBel, A., & D’Mello, A. M. (2025). Ignoring the cerebellum is hindering
1151 progress in neuroscience. *Trends in Cognitive Sciences*, 29(4), 318–330.
1152 <https://doi.org/10.1016/j.tics.2025.01.004>
- 1153 Wolpert, D. M., Miall, R. C., & Kawato, M. (1998). Internal models in the cerebellum.
1154 *Trends in Cognitive Sciences*, 2(9), 338–347. [https://doi.org/10.1016/S1364-](https://doi.org/10.1016/S1364-6613(98)01221-2)
1155 [6613\(98\)01221-2](https://doi.org/10.1016/S1364-6613(98)01221-2)
- 1156 Yamazaki, T., & Tanaka, S. (2009). Computational Models of Timing Mechanisms in the
1157 Cerebellar Granular Layer. *The Cerebellum*, 8(4), 423–432.
1158 <https://doi.org/10.1007/s12311-009-0115-7>
- 1159 Zhang, Y., Brady, M., & Smith, S. (2001). Segmentation of brain MR images through a
1160 hidden Markov random field model and the expectation-maximization algorithm.

1161 *IEEE Transactions on Medical Imaging*, 20(1), 45–57.

1162 <https://doi.org/10.1109/42.906424>

1163

1164 **Figure legends**

1165 **Figure 1.** a) Task schematic. Example stimuli pictured in **Supplemental Figure 1.** b)
1166 Anatomical ROI masks. c) Learning curve and model fit. d) Choice and RT performance on
1167 short and long delay trials. e) Gaze on nonrewarded (+0) versus rewarded (+1) trials. Larger
1168 values depict data from whole trial and smaller values depict data during the feedback phase
1169 only. f) Respiration and pulse rates on rewarded versus nonrewarded trials.

1170

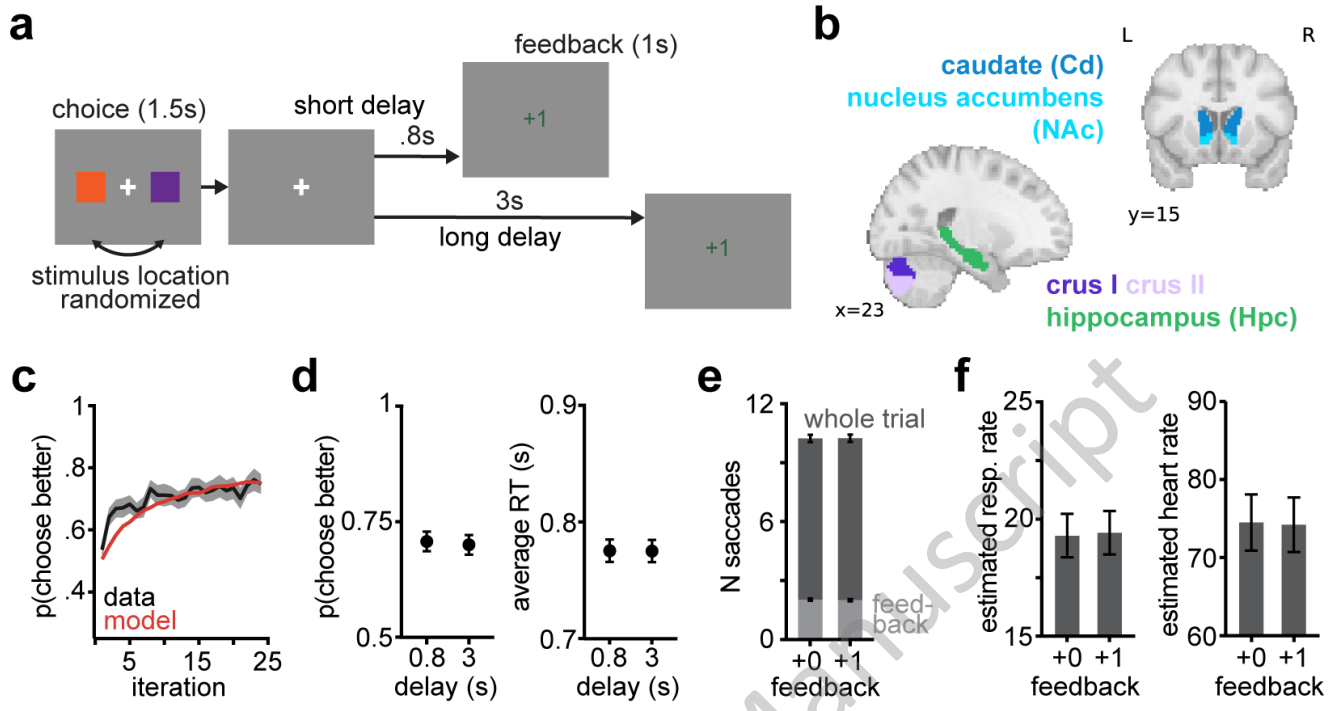
1171 **Figure 2.** a) Contrast of activity on rewarded versus nonrewarded trials at the point of feedback
1172 in the whole brain (left panel) and in cerebellum (right panel; plotted on cerebellar flat map, see
1173 Methods). Whole brain result is cluster-corrected at $p < .001$. Cerebellar results are cluster-
1174 corrected in cerebellum, $p < .001$. b) Rewarded > nonrewarded contrast at short and long delays
1175 in cerebellum (cluster-corrected in cerebellum, $p < .001$). c) Contrast of activity for rewarded >
1176 non-rewarded trials in cerebellar (Crus I and II), striatal (Nucleus Accumbens, NAc; Caudate
1177 Nucleus, Cd), and hippocampal (Hpc) ROIs. ** $p < .001$; * $p < .05$

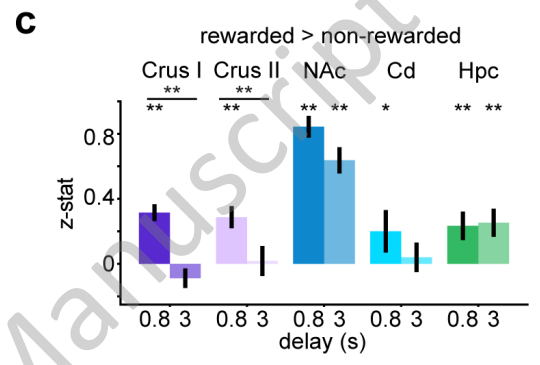
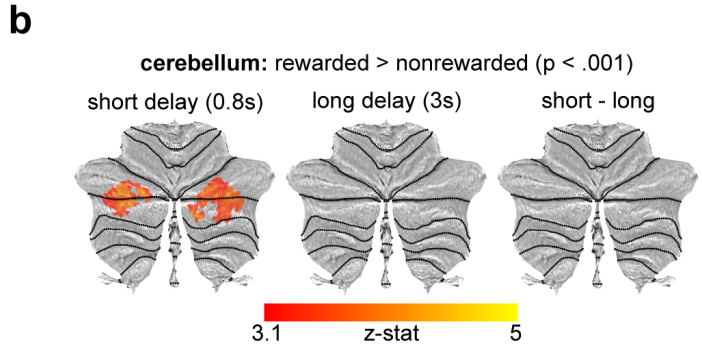
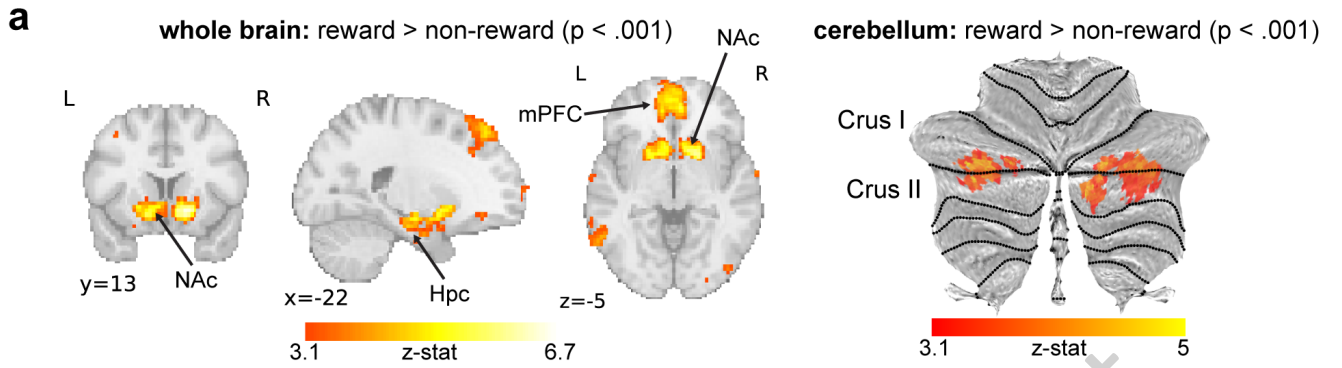
1178 **Figure 3.** a) Schematic of model-based fMRI approach. b) Reward Prediction Error (RPE)
1179 responses (whole brain cluster-corrected, $p < .001$). and cerebellum (cluster-corrected in
1180 cerebellum, $p < .001$). c) RPE response on rewarded trials at short and long feedback delays
1181 (cluster-corrected in cerebellum, $p < .001$). d) RPE responses at short and long delays in
1182 cerebellar and other subcortical ROIs. ** $p < .001$; * $p < .05$

1183 **Figure 4.** a) Whole-brain analysis showing voxels where short RPE > long RPE contrast covaries
1184 with performance on short delay trials. (cluster-corrected in whole brain, $p < .05$). b) Same analysis
1185 restricted to cerebellum (cluster-corrected in cerebellum, $p < .001$). c) Visualization of the correlation
1186 between activity in the significant cluster in the cerebellum from panel b, and learning performance
1187 for short delay stimuli.

1188 **Figure 5.** a) Illustration of PPI analysis. b) PPI analysis results seeded in Crus I (red regions
1189 cluster-corrected at $p < .01$). c) PPI analysis results seeded in Crus II (red cluster-corrected at p
1190 $< .01$, yellow at $p < .001$).

JNeurosci Accepted Manuscript





JNeurosci Accepted Manuscript

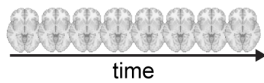
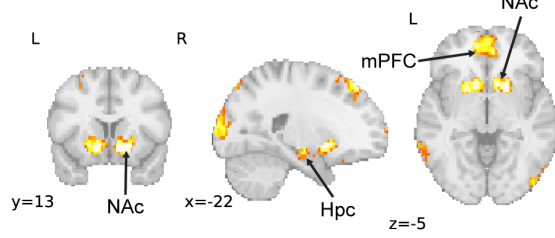
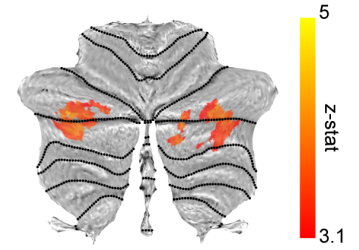
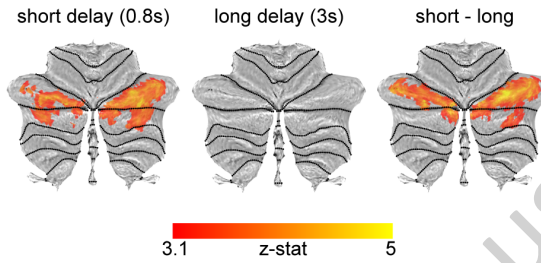
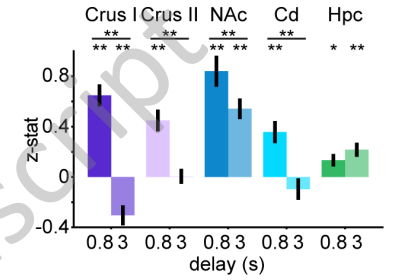
a**1. Fit RL models to data****learning rule**

$$Q_{t+1}(s) = Q_t(s) + \alpha \text{RPE}_t$$

$$\text{RPE}_t = \text{reward}_t - Q_t(s)$$

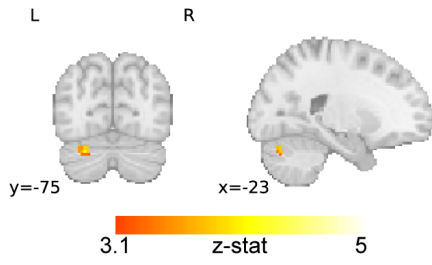
choice policy

$$p(s) = \frac{e^{Q(s)\beta}}{\sum e^{Q(s)\beta}}$$

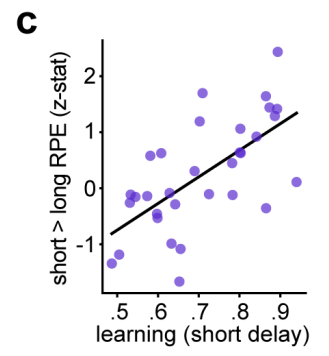
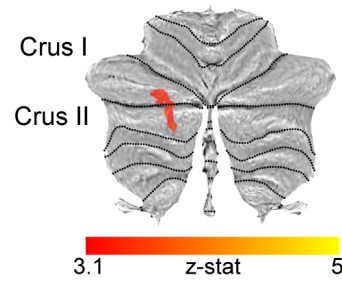
2. Simulate trial-by-trial RPEs**3. Regress against BOLD data****b****whole brain: RPE (p < .001)****cerebellum: RPE (p < .001)****c****cerebellum: RPE (p < .001)****d****RPE responses**

JNeurosci Accepted Manuscript

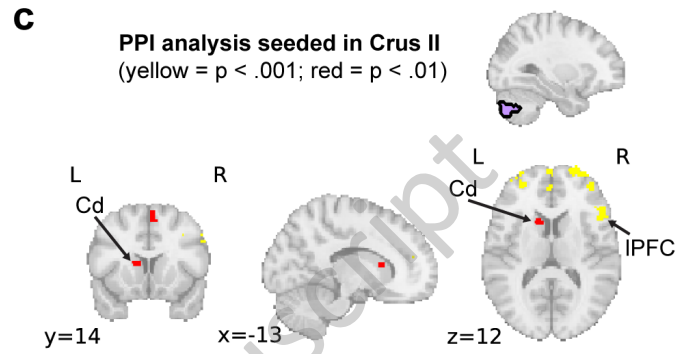
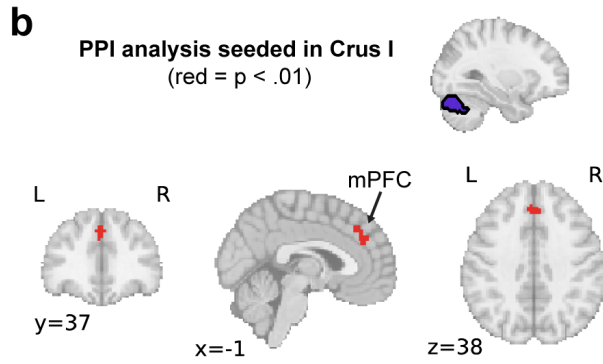
a short RPE > long RPE x performance
($p < .05$)



b short RPE > long RPE x performance
($p < .001$)



JNeurosci Accepted Manuscript



JNeurosci Accepted Manuscript